Linköping University | Department of Management and Engineering
Master's thesis, 30 credits | Applied mechanics
Spring 2023 | LIU-IEI-TEK-A–23/04609–SE

Structural responses due to underwater detonations

Validation of explosion modelling methods using LS-DYNA

Ebba Carlsson
Gustav Blomgren

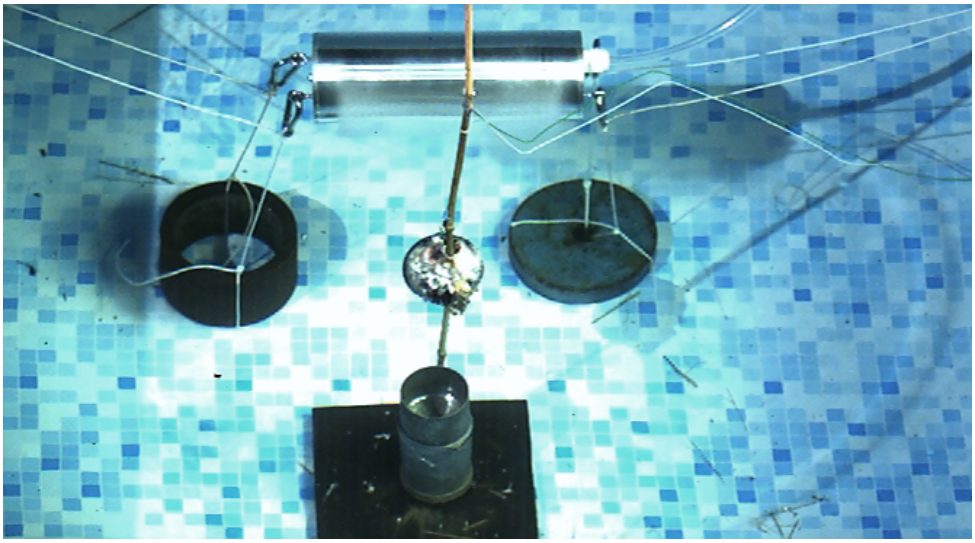

LINKÖPING UNIVERSITY

Linköping University
SE-581 83 Linköping, Sweden
+46 13 28 10 00, www.liu.se

Abstract

Modelling the full event of an underwater explosion (UNDEX) is complex and requires advanced modelling methods in order to achieve accurate responses. The process of an UNDEX includes a series of events that has to be considered. When a detonation is initiated, a shock-wave propagates and the rest products from the explosive material creates a gaseous bubble with high pressure which pulsates and impacts the surroundings. Reflections of the initial shock-wave can also appear if it hits the sea floor, water surface or other obstacles.

There are different approaches how to numerically model the impact of an UNDEX on a structure, some with analytical approaches without a water domain and others where a water domain has to be modelled. This master's thesis focuses on two modelling methods that are available in the finite element software LS-DYNA. The simpler method is called Sub-Sea Analysis (SSA) and does not require a water domain, thus it can be beneficial to use in an early design stage, or when only approximated responses are desired. To increase the accuracy, a more complex method called S-ALE can be used. By implementing this method, the full process of an UNDEX can be studied since both the fluid domain and explosive material are meshed. These methods are studied separately together with a combination of them.

Another important aspect to be considered is that oscillations of a structure submerged in water differs from the behavior it has in air. Depending on the numerical method used, the impact of the water can be included. Natural frequencies of structures submerged in water are studied, how it changes and how the methods takes this into account.

To verify the numerical models, experiments were executed with a cylindrical test object where the distance and weight of charge were change throughout the test series. It was found that multiple aspects affects the result from the experiments, these aspects are not captured in the numerical models. These aspects have for instance to do with reflections, how accurate the test object is modelled and the damping effects of the water.

It is concluded that the numerical models are sensitive when small charges and fragile structures are studied. High frequency oscillations were not triggered in the experiment but found for both methods. It should be further investigated if the methods are more accurate for larger charges and stronger structures. Experiments with larger water domain would also be beneficial to remove reflections as well as a more accurate model of the cylinder in the simulations.

Acknowledgements

We would like to thank our supervisor Mikael Holmgren at Saab Dynamics in Linköping for all the support and helpful advice during the spring. Similarly, we appreciate our manager Hans Bergman for giving us this opportunity and believing in our abilities. We also want to express our gratitude to our supervisor Daniel Leidermark and examiner Jonas Stålhand at Linköping University for the support during the master's thesis.

A special thanks to Jenny Lundgren who helped us with the construction of the test object and Nils Hjertner for manufacturing it and providing us with components. Also, thanks to David Fyhrman and David Aspenberg at Dynamore Nordic AB for providing us with all the valuable support in LS-DYNA.

Lastly, we would like to thank Torbjörn Östin and Mikael Strohmaier at Saab Dynamics AB in Karlskoga for helping us with the execution of the experiments and the preparations for it.

Nomenclature

Abbreviations and Acronyms

Abbreviation	Meaning
ALE	Arbitrary Lagrangian Euler
BC	Boundary condition
BEM	Boundary element method
DAA	Double Asymptotic Approximation
EOS	Equations of State
FE	Finite element
FSI	Fluid Structure Interaction
MMALE	Multi Material Arbitrary Lagrangian Euler
SSA	Sub-Sea Analysis
S-ALE	Structured - Arbitrary Lagrangian Euler
UNDEX	Underwater Explosion
USA	Underwater Shock Analysis

Keywords

Keyword	Description
*ALE_STRUCTURED_FSI	Defines FSI coupling for S-ALE and solid part
*ALE_MULTI-MATERIAL_GROUP	Defines multi-material group for ALE
*ALE_STRUCTURED_MULTI-MATERIAL_GROUP	Defines multi-material group for S-ALE
*ALE_STRUCTURED_MESH_VOLUME_FILLING	Fills the S-ALE mesh with multi-material groups
*CONSTRAINED_LAGRANGIAN_IN_SOLID	Defines FSI coupling for ALE and solid part
*CONTROL_IMPLICIT_GENERAL	Defining implicit/explicit solver
*CONTROL_IMPLICIT_EIGENVALUE	Defining settings for eigenvalue study
*HIGH_EXPLOSIVE_BURN	Defines the explosive material
*INITIAL_DETONATION	Defines the initialisation of detonation
*INITIAL_VOLUME_FRACTION_GEOMETRY	Fills the ALE mesh with multi-material groups
*MAT_24	Defines piecewise-linear elasto-plastic material

Greek symbols

Symbol	Description	Unit
δ_{ij}	Kronecker delta	[-]
θ	Decay constant	[ms]
μ	Parameter for EOS	[-]
γ_0	Gruinisen gamma	[-]
ρ	Relative density	[kg/m^3]
σ_r	Stress in radial direction of shell	[MPa]
σ_x	Stress in axial direction of shell	[MPa]
σ_φ	Stress in tangential direction of shell	[MPa]
σ_{ij}	Cauchy stress tensor	[MPa]
ω	Parameter for JWL	[-]

Latin symbols

Symbols	Description	Units
a, C, S_1, S_2, S_3	Parameters for Gruneisen	[-]
A, B, R_1, R_2	Parameters for JWL	[-]
A1, A2, K1, K2, K3, K4	Parameters for explosive material	[-]
C_0, C_1, C_2, C_3, C_4, C_5, C_6	Parameters for Linear Polynomial	[-]
D	Depth	[m]
E	Internal energy density per unit initial volume	[-]
h	Wall thickness of cylindrical shell	[m]
P(t), P	Pressure	[MPa]
P_0	Maximum Pressure	[MPa]
r	Middle radius of cylindrical shell	[m]
R	Distance from detonation to point of interest	[m]
R_{max}	Maximum bubble radius	[m]
t	Time after shock-wave arrive at point of interest	[ms]
T	Time until maximum bubble radius occurs	[s]
$\mathbf{v}$	Velocity vector	[m/s]
V	Relative volume	[-]
W	Weight of explosive charge	[kg]

Contents

1 Introduction **2**
- 1.1 Objectives and deliverables . . . 2
- 1.2 Delimitations . . . 3
- 1.3 Other considerations . . . 3

2 Underwater detonations **4**
- 2.1 Shock-wave . . . 4
- 2.2 Gas bubble . . . 5
- 2.3 Reflection and cavitation . . . 6

3 Structural responses **8**
- 3.1 Plastic material model . . . 8
- 3.2 Natural frequencies . . . 9

4 Modelling underwater detonations **10**
- 4.1 Element formulation . . . 10
- 4.2 Equation of state (EOS) . . . 11
- 4.3 Solvers for UNDEX . . . 12
  - 4.3.1 Sub-Sea Analysis (SSA) and Underwater Shock Analysis (USA) . . . 12
  - 4.3.2 Lagrangian element formulation . . . 13
  - 4.3.3 Arbitrary-Lagrangian-Euler (ALE) . . . 13
- 4.4 Fluid Structure Interaction (FSI) and Boundary Element method (BEM) . . . 14

5 Methodology **15**
- 5.1 Experiments . . . 16
- 5.2 Earlier work for validation . . . 19
- 5.3 Numerical model of test object . . . 20
- 5.4 Sub-Sea Analysis (SSA) . . . 21
- 5.5 Multi-physical analysis with S-ALE . . . 21
  - 5.5.1 Multi-physical analysis with SSA . . . 22
  - 5.5.2 Multi-physical analysis with full detonation process . . . 23
  - 5.5.3 Mesh verification S-ALE . . . 23
- 5.6 S-ALE performance . . . 26
- 5.7 Natural frequencies . . . 27

6 Results and Discussion **28**
- 6.1 Analytical validation . . . 28
- 6.2 Natural frequencies . . . 28
- 6.3 Experiments . . . 31
  - 6.3.1 Pressure validation for analytical calculations and S-ALE . . . 31
  - 6.3.2 Strain response for Case 1:3 . . . 32
  - 6.3.3 Strain comparison of Case 1:4 and 3:2 . . . 33
  - 6.3.4 Bubble impact for Case 1:5 . . . 34
  - 6.3.5 Plastic deformation for Case 2:5 . . . 36
  - 6.3.6 Further implementation of SSA . . . 38
  - 6.3.7 Studied modelling approaches for Case 3:3 . . . 39

7 Conclusions and Future work **41**
7.1 Conclusions 41
7.2 Future work 41

References **43**

1 Introduction

This master's thesis is carried out at Saab Dynamics AB in Linköping, Sweden. Saab develops and manufacture defense material used for both air and underwater applications. Underwater products such as mine sweepers and torpedoes, operate under water where they are at risk of being in the vicinity of explosions that can damage or disturb them. How explosions behave and propagate under the water surface are different to above the surface. Thus it is of great importance to simulate and analyse the behaviour of underwater explosions (UNDEX). With increased knowledge about UNDEX, structural responses in solid objects can be analysed. A better understanding of the structural responses will assist in setting criterias for components in underwater products. Below in Fig 1.1 is a simplified visualisation showing the case that this master's thesis work will contain. It includes experiments of a cylinder subjected to an UNDEX. The result is then used to compare and calibrate numerical models.

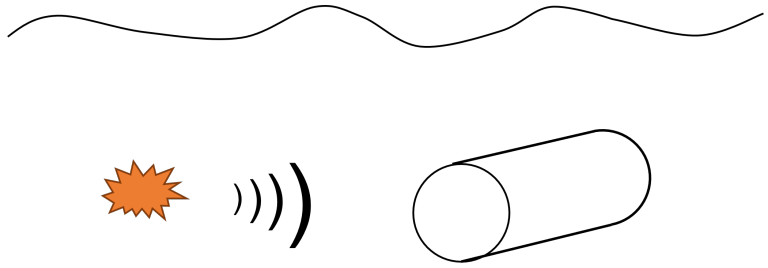

Fig 1.1: Simplified view of the studied case. A cylinder subjected to an UNDEX.

1.1 Objectives and deliverables

For this master's thesis work, it is desired to predict the responses of a solid structure subjected to an UNDEX. In order to receive predictions with good accuracy for the structural response, modelling of the surrounding fluids has to be accurate. It is therefore included how to model the event of an UNDEX. The structural response includes frequency study, plastic deformation and acceleration levels.

The objective is to analyse a structure subjected to an UNDEX by using multiple modelling methods. The work is divided in parts, where the complexity of the numerical models increase. The most complex model includes initiation of detonation, shock-wave propagation, bubble pulse and reflections. All models are compared to experiments in order to conclude the accuracy of each model and how it can be used during a design process. Earlier work complement the experiments in the validations.

1.2 Delimitations

Simulating an UNDEX is complex and a variety of methods can be used in consideration of different levels of accuracy. Two bases of different modelling approaches will be studied in this master's thesis. These approaches are a fluid domain-free method called Sub-Sea Analysis (SSA) and a multi-material based mesh domain including interaction between fluid and structure in the finite element software LS-DYNA. This method will later be presented as S-ALE. Combinations of these methods and modifications to improve the accuracy are studied as well.

A cylinder is used as a generic geometry to widen the applicability of the results while not making the numerical model too complex. The numerical method and model set-up is the predominant objective in contrast to an exact geometry. This master's thesis should therefore include guidelines for how to accurately model an UNDEX and the structural responses for an object subjected to it.

The experiments are limited to be down-scaled compared to the products developed at Saab Dynamics AB. This work will be a first trial of executing such experiments, thus they can probably be further improved when applying it on a larger scale.

1.3 Other considerations

No gender related issues are brought up by this work. Neither is there any direct connection to questions related to environmental or sustainability in community development. In regards to ethical considerations, this master's thesis involve defense material that are in line with Swedish law.

2 Underwater detonations

In contrast to air, more pressure is needed to compress water and it is often, for simplicity, treated as incompressible. There are also more complex phenomena appearing beside a first shock-wave. After initialisation of an UNDEX, a shock-wave forms and propagates symmetrically in the time frame of milliseconds while a gas bubble forms, grows and collapses in the time frame of seconds. If the UNDEX is initiated in shallow water, or close to the water surface/bottom, the initial shock-wave will reflect at these surfaces. This can affect the structure with secondary shock-waves which may contribute to further damage of the structure. [1]

2.1 Shock-wave

Reid [2] describes that when the detonation occurs in water, the pressure shock-wave travels with a velocity greater than the speed of sound. The velocity of the shock-wave quickly decreases and stabilises at the speed of sound in water. Constanzo [1] states that the pressure generated by a shock-wave starts at the maximum value and then decreases exponentially with time once the shock-wave has reached the point or object of interest. The time it takes for the pressure to decrease to 37% of the maximum value is called the decay constant, θ. This primary shock-wave will be a compressive shock-wave, meaning that the pressure is raised across the shock front as the shock-wave passes through the fluid. The pressure in the shock-wave can be expected to follow the exponential behaviour until the decay constant is reached, after this the decay of the pressure slows down. The propagation of the initial shock-wave is visualized in Fig 2.1.

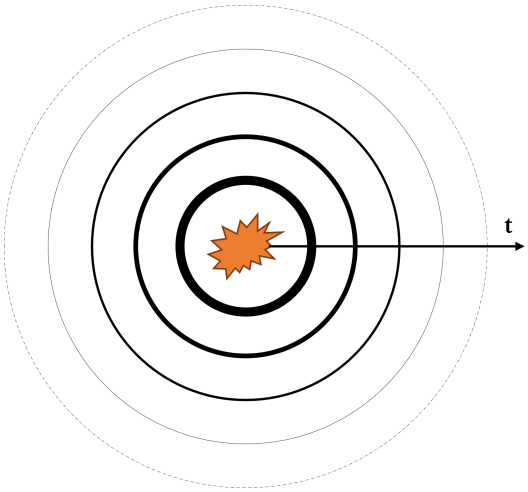

Fig 2.1: Propagation of primary shock-wave during time t.

The pressure depends on the time t up until it reaches the decay constant in the following way [1]:

$$\mathrm{P(t)} = \mathrm{P_0} \cdot \mathrm{e}^{-\mathrm{t}/\theta} \quad 0 \leq \mathrm{t} \leq \theta \tag{2.1}$$

where $\mathrm{P_0}$ is the time independent peak shock-wave pressure. The time t is from when the shock-wave reaches the measuring point, thus $\mathrm{P(t)} = \mathrm{P_0}$ at time t=0. $\mathrm{P_0}$ will approximately decrease linearly with respect to the distance from the detonation point (R). This holds outside a sphere centered at the detonation point with a radius three times the radius of the explosive charge. Inside this radius, the maximum pressure will not decrease linearly. [1]

The shock-wave behaviour depends on the weight of the explosive charge (W) and the distance between the detonation point and pressure-measuring point (R). The maximum shock-wave pressure P_0 can be calculated by [2]:

$$P_0 = K1 \cdot (W^{1/3}/R)^{A1} \quad K_1, A_1 > 0 \tag{2.2}$$

where K1 and A1 are material parameters for the explosive material. The expression for the decay constant θ is

$$\theta = K2 \cdot W^{1/3} \cdot (W^{1/3}/R)^{A2} \quad K_2, A_2 > 0 \tag{2.3}$$

and depends on the explosive material parameters K2 and A2. [2]

2.2 Gas bubble

Because of high temperature and pressure during the explosion, a gas bubble forms from the detonation point, and expands and compresses in cycles. The expansion occurs until the pressure inside the bubble becomes lower than the pressure in the surrounding water. Because of the high outward momentum of the bubble growth, the pressure in the bubble reaches lower levels than the surrounding fluid. When the pressure gradient is large enough, the bubble stops expanding and compresses. The bubble compresses until the gasses inside cannot be compressed further, an over-pressure is reached and the bubble expands again. A sequence of the bubble expansion and compression is demonstrated in Fig 2.2. It is shown that the pressure is mostly negative, i.e. under the hydro-static pressure at that specific water-depth. The pressure rises when the bubble compresses as seen in the pressure graph. It is also shown that the bubble moves upwards towards the water surface. This is due to gravitational and buoyancy forces that overcomes the drag force on the bubble in the fluid. The cycles of the bubble continues until it reaches the water surface, or for a deep sea explosion until the energy of the bubble has dissipated. Because of loss in energy, the maximum size of the bubble decreases with cycles and the minimum size, at compression, increases. [1]

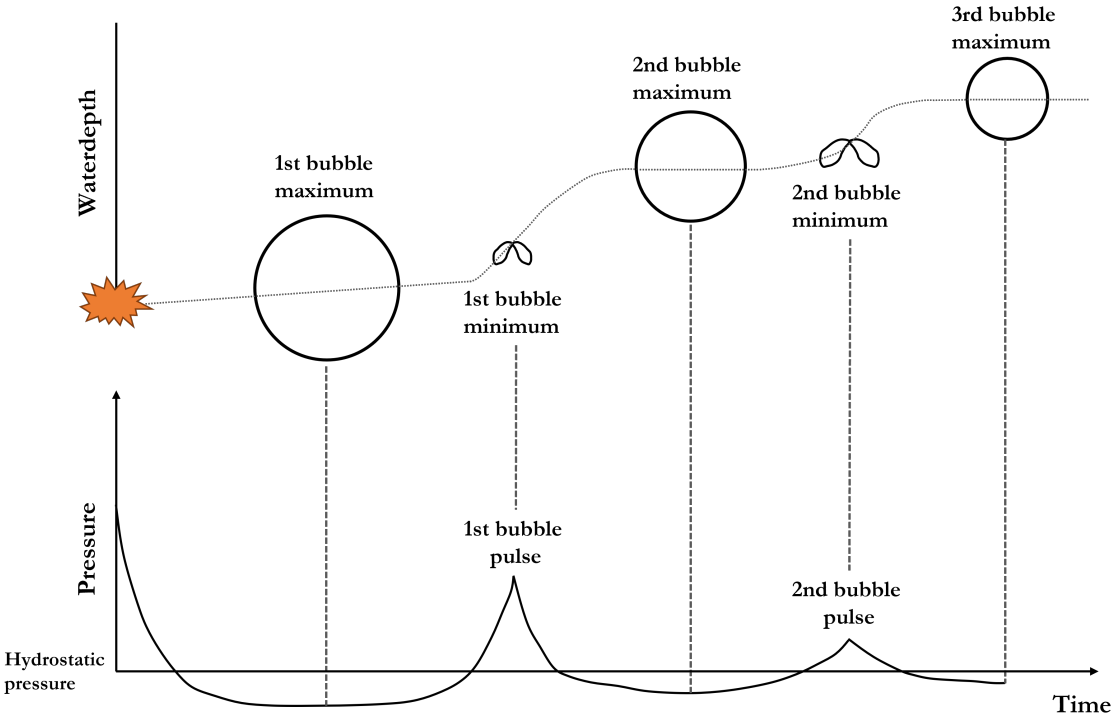

Fig 2.2: Sequence of bubble expansion and compression. The figure is inspired by Constanzo [1].

Structures that are in range of the effects from the gas bubble can be extensively damaged by the bubble. With a bubble pulsating at a distance from the object, the frequency of the pressure pulses can lead to natural frequency responses. A structure can also be directly damaged by the bubble if it expands closely. Lastly, the bubble can also collapse close to a structure which can cause cavitation and further water jet penetration damage. Comparing the peak pressures for the primary shock-wave and bubble collapse, the bubble's peak pressure reaches around 10% of the primary shock-waves peak pressure. Size of the explosive material and depth of the detonation in water impacts the size of the bubble. [2]

The expression for maximum bubble radius reads [2]:

$$R_{max} = K6 \cdot (W^{1/3}/(D + 9.8))^{1/3} \quad K_6 > 0 \tag{2.4}$$

where K6 is a material parameter and D is the depth of the explosive mass. The time for the first bubble pulse, at which the bubble reaches its minimum radius during the first cycle is expressed by [2]:

$$T = K5 \cdot (W^{1/3}/(D + 9.8)^{5/6}) \quad K_5 > 0 \tag{2.5}$$

where K5 is a material parameter.

2.3 Reflection and cavitation

After the detonation, a compressive direct shock-wave will propagate through the water and can reach the water surface or the sea floor. When reaching the water surface, the difference in impedance between the water and air will cause a reflection of the shock-wave back down into the water. The reflected shock-wave is tensile and reduces the pressure across the shock-front. The time between the direct compressive shock-wave and the reflected tensile shock-wave is called surface cut-off time. The shock-wave can also be reflected in the sea floor, and depending on the material of the sea floor, it can either be a strong compressive reflection or a weak tensile reflection. [1]

How reflections can propagate through the water and affect a structure is shown in Fig 2.3. The structure is subjected to both a direct shock-wave and reflected waves from water and bottom surfaces.

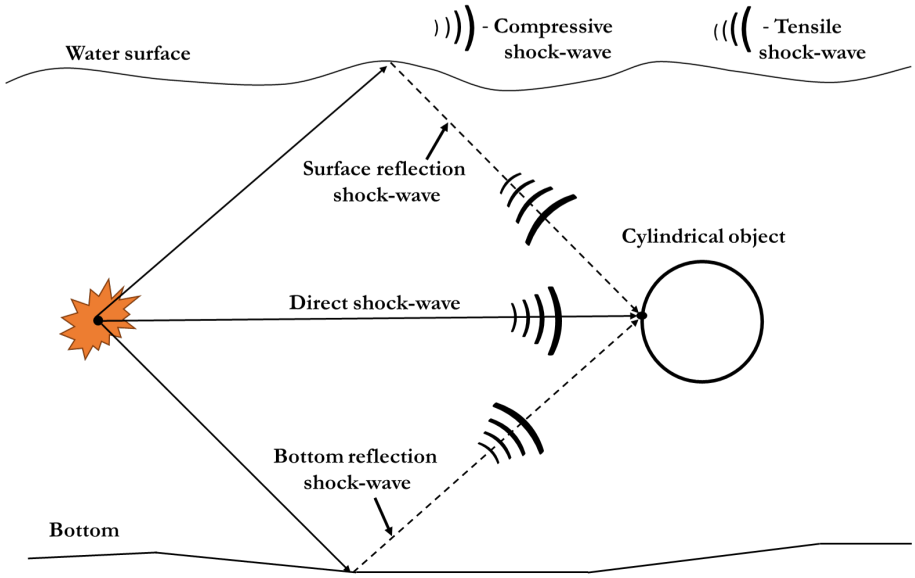

Fig 2.3: Schematic view of how reflections from UNDEX can affect a structure. The figure is inspired by Constanzo [1].

Tensile waves reflected at the water surface contributes to cavitation since water is incapable of handling large tension. The fluid will go from a homogeneous liquid to a cavitated non-homogeneous medium with regions containing vapour. These cavitations are unable to transmit any shock-waves and closes as a consequence of gravity, pressure and flow direction. When the cavitations collapses, two masses of fluid (from each respective side of the cavitation region) will collide creating a shock-wave/compressive pulse. This is known as the bulk cavitation closure pulse. This pressure pulse is generally significantly smaller than the primary compressive pressure pulse and the bubble collapse pressure pulse, but there are exceptions. [1]

3 Structural responses

A cylinder exposed to an UNDEX can have a variety of responses. Because of high pressure from the shock-wave, the material can deform plastically and become damaged. As mentioned earlier, the pulsation of the bubble can match the natural frequencies of the structure. This could lead to damage of components, or a whole structure. The background to the structural responses is presented within this section.

If a thin walled cylindrical structure is exposed to an external pressure, there is a risk of buckling. For stable and evenly distributed over-pressures, formulas exist that predict the critical load [3]. For the case of an explosion, the very sudden burst of non-uniform over-pressure makes these formulas unreliable. Instead focus will be put on conventional stress and strain responses when analysing the structural loads.

When an object is hit by a shock-wave from an UNDEX, it will for a brief time, be accelerated and move due to the uneven pressure applied. The magnitude of the acceleration depends on a variety of factors: how much of the shock-wave energy is absorbed by deformations, how much resistance to movement the surrounding fluid gives, and what moment of inertia the structure has. It is therefore hard to analytically calculate the acceleration levels from an UNDEX. No focus is put on analytical calculations for acceleration, but both simulation and experimental results are examined and presented.

The coordinate system of a cylinder is shown in Fig 3.1. Because of its thin wall, the radial stress will be negligible.

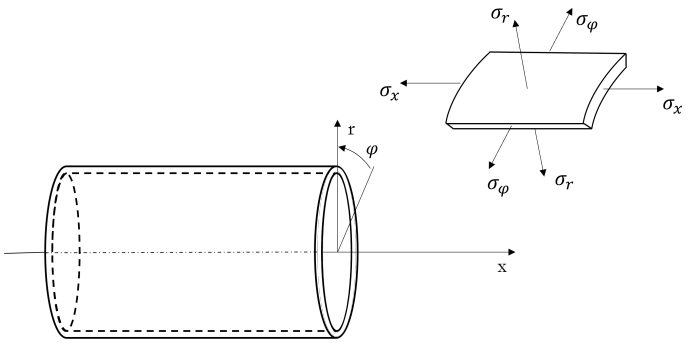

Fig 3.1: Cylinder with the coordinate system defined. The direction of stresses in an element in the cylinder is shown to the right. The figure is inspired by [3].

3.1 Plastic material model

There is a large amount of material models in LS-DYNA, developed for a variety of applications and materials. To account the plastic responses of the cylinder, a material model with plasticity formulation is needed. The material model Piecewise-Linear-Plasticity (*MAT_24) is simple to use when mechanical material properties are defined. One can use the *keyword*-card to define different plasticity processes.

Perfect plasticity is received if the tangent modulus is set to a small value. One can also receive linear-plastic behaviour by setting a constant value for tangent modulus. In order to define hardening behaviour correlated to real values, a stress-strain curve containing data points can be imported, giving a piecewise-linear repsonse. With a large amount of data points, the plasticity behavior becomes approximately non-linear. The curve is defined for true stress and true plas-

tic strain, up to the maximum stress the material can withstand before relaxation and further damage. The three mentioned ways of defining a stress-strain curve is shown in Fig 3.2. The material model allows strain rate-dependency, but that requires a material curve for different strain rates. [4]

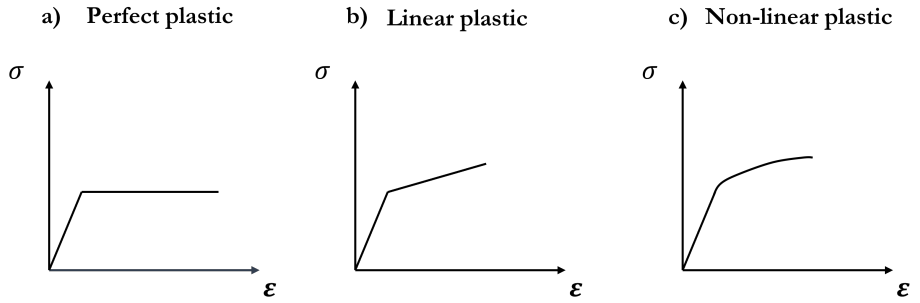

Fig 3.2: Stress-strain curve for a) perfect plastic, b) linear plastic and c) non-linear piece-wise plastic hardening. The figure is inspired by [4].

The pressure found from the material model is calculated from the stresses and is therefore representing the pressure within the structure's elements. In comparison, the analytical expression (from Eq 2.1) gives the pressure of the shock-wave and not the structural response. These ways of extracting pressure will therefore not correspond, which is why the analytical pressure will be converted to stress by the assumption of a thin walled closed cylinder [3], when comparing it to stress responses of a structure.

$$\sigma_{\varphi} = \frac{\mathrm{P\ r}}{\mathrm{h}} \tag{3.1}$$

h is the wall thickness and r the middle radius of the cylinder.

3.2 Natural frequencies

When studying natural frequencies of a structure submerged in water, mass can be added to the structure in order to account for the effect from the fluid [5]. In air, this is rather simple, due to the low mass of displaced air in relation to the mass of the structure. The displaced mass is greater in water, thus it has to be considered when calculating the natural frequencies. The level of natural frequencies will generally be lower in a wet condition compared to dry. Sarpkaya [5] brings up an assumption which says that due to the water, the added mass can be approximated as the inviscid flow value. It is noted that this is not similar to the displaced mass of the fluid. There is no clear statement of how the inviscid flow value is defined. It is, although, concluded that the characteristics of the flow over a body has an impact on the natural frequencies. An example about flow around a plate is brought up. An approximation is that the added mass for a vertical oriented thin plate can be defined by a cylinder enveloping the plate. If the plate, on the other hand is oriented horizontally, the added mass will be zero.

4 Modelling underwater detonations

During the event of an UNDEX, there is more than one material present. The fluid domain contains air, water, explosive material and additional gaseous products in the bubble that are formed from the detonation. There is also a possibility of cavitation which represents an additional medium in the form of vacuum. Together with this, there is also the solid structure placed in the fluid domain. [6]

Underwater detonations can be modelled by a variety of methods, some with a more analytical approach than others. When considering the opportunities in LS-DYNA, the simplest way of setting up a model is by using SSA. Without modelling a water domain, responses on a structure can be calculated. This method will be described further within this section. There are also ways of modelling multi-material domains with the Arbitrary Lagrangian Eulerian method (ALE). This is also further described in this section. Before that, different element formulations are described, as well as equations of state needed when modelling fluid and explosive materials.

4.1 Element formulation

In numerical solvers, different descriptions of flow motion are available. As seen in Fig 4.1, Eulerian formulation contains a fixed spatial, mesh and mass fluxes over element boundaries are calculated. This formulation is usually preferred for large deformations such as motion of fluids. Another description is the Lagrangian formulation where the nodes are connected to the material. This formulation is typically used in solid materials with small deformations. Lagrangian meshes can suffer from large element distorsions, since the elements remains fixed to the material. If this formulation is used for fluids, large distortions of elements can be reduced by limiting time step size but this can instead lead to expensive calculations. For problems including multiple fluids, solvers have been developed which combines Eulerian and Lagrangian element formulations. One of those solvers is ALE and it uses one coordinate system to couple the dynamics of all fluids and is the most efficient method for solving UNDEX. [6]

As it can be seen for the Lagrangian formulation in Fig 4.1, the elements are distorted to a larger extent than for the ALE element formulation. ALE minimizes the distortion of elements by using both Eulerian and Lagrangian formulation.

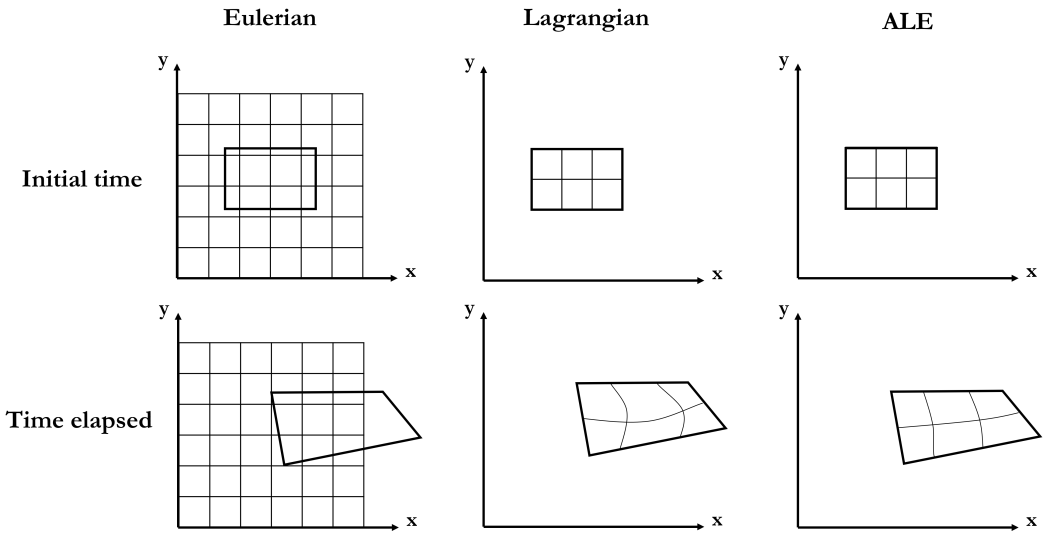

Fig 4.1: Different element formulation described schematically.

4.2 Equation of state (EOS)

When modelling materials, it is for some cases necessary to introduce equations of state. With such description, the thermodynamic state of the material is related in terms of, for example, pressure and internal energy. A variety of equations of states are available, each more or less suited for a certain material class. For this master's thesis, EOS has to be defined when modelling fluid and explosives with ALE.

Three definitions for EOS have been described and used by Sjöstrand [7] and Otsuka et al. [8]. These are Linear Polynomial, Gruneisen and Jones-Wilkens-Lee (JWL). Different EOS descriptions are applied to different fluids, in order to have accurate formulations for the states of the fluids. Linear Polynomial is usually used for air, but can also be applied for water. Otsuka et al. and Sjöstrand used it for air, and Sjöstrand studied it for water as well. Gruneisen is another description that was used for water in both of the earlier studies. Sjöstrand did not find any extensive differences when using Linear Polynomial or Gruneisen for water. For the explosive material, JWL was used in both studies and it has to be defined together with the *keyword* *HIGH_EXPLOSIVE_BURN. The definitions for the EOS introduced are found from [9].

The expression for the pressure in the Linear Polynomial description is:

$$P = C_0 + C_1\,\mu + C_2\,\mu^2 + C_3\,\mu^3 + (C_4 + C_5\,\mu + C_6\,\mu^2)\,E, \tag{4.1}$$

where the parameters C_0 to C_6 are positive material dependent and E the internal energy density per unit initial volume. The parameter μ is defined as

$$\mu = \frac{1}{V} - 1 \tag{4.2}$$

where V is the relative volume, i.e. the ratio of the current to the initial volume of an element. For Gruneisen, pressure for compressed material is calculated as

$$P = \frac{\rho_0\,C^2\,\mu\left[1+\left(1-\frac{\gamma_0}{2}\right)\mu - \frac{a}{2}\,\mu^2\right]}{\left[1-(S_1-1)\mu - S_2\,\frac{\mu^2}{\mu+1} - S_3\,\frac{\mu^3}{(\mu+1)^2}\right]^2} + (\gamma_0 + a\mu)\,E\,. \tag{4.3}$$

The equation refers to a curve of the cubic shock velocity and particle velocity ($u_s - u_p$ curve). C is the interception of the $u_s - u_p$ curve and S_1, S_2 and S_3 are slope coefficients. γ_0 is the Gruneisen gamma, and a the first order volume correction to γ_0. All of these parameters can be defined by the user within the *keyword*-card. V is defined as in Eq (4.2). For expanded material, pressure is defined as

$$P = \rho_0\,C^2\,\mu + (\gamma_0 + a\mu)\,E\,. \tag{4.4}$$

For the explosive material, pressure is defined as follows for JWL description

$$P = A\left(1 - \frac{\omega}{R_1 V}\,e^{-R_1 V}\right) + B\left(1 - \frac{\omega}{R_2 V}\,e^{-R_2 V}\right) + \frac{\omega E}{V} \tag{4.5}$$

where A, B, R_1, R_2 and ω are constant material parameters.

4.3 Solvers for UNDEX

There are multiple methods to model the event of an UNDEX and they are more or less complex with varying degree of accuracy. Which method to use depends on the objective, for example solving the bubble pulse or only the structural response.

Due to the multi-physical characteristics of modelling within this field, a way of modelling both structure, explosive and surrounding medium has do be considered. Three types of solvers for this type of applications in LS-DYNA are:

- Methods with no fluid domain: Sub-sea Analysis (SSA) and Underwater Shock Analysis (USA)
- Coincident meshing of Lagrangian elements used for modelling both structure and water
- Arbitrary-Lagrangian-Euler (ALE) which combines Eulerian and Lagrangian characteristics in the elements representing water and couples them to Lagrangian elements representing a structure using a penalty based algorithm.

4.3.1 Sub-Sea Analysis (SSA) and Underwater Shock Analysis (USA)

There are methods for simulating UNDEX without modelling a fluid domain, and one is SSA. With this algorithm it is possible to account for direct shock-wave and bubble oscillations without generating a mesh for the water domain. Settings needed for the *keyword* contains position, dimensions and material properties of the explosive material. Dimensions of the fluid in terms of water-depth and distance to the water surface has to be defined together with general fluid properties. It is possible for the user to decide if reflections from the sea floor should be included. Further, flooding status has to be prescribed for the objects subjected to the effects of the detonation. There are four different choices which describes if there are fluid or air inside and outside the object. This information is used by the solver when pressure is applied on the structure. [9]

The algorithm uses the same expressions for peak pressure, pressure over time and decay constant as provided in Section 2.1. It is not possible to receive pressure outputs from any other location than on the structure and it is therefore not possible to compare the shock-wave propagation and bubble oscillations with other modelling approaches that includes a fluid domain.

Studies with SSA have been carried out by Sjöstrand [7] and Nawa and Just [10]. The approaches differ slightly where Sjöstrand only uses a cylindrical structure and detonates explosive material 1.8 m away. Nawa and Just studies a part of a cylinder, but also has an additional layer of solid elements on top of the structure. These elements are modelled as water. On top of this, one more layer of shell elements are modelled with no stiffness applied. According to Nawa and Just, this is necessary in order to receive a correct application of load onto the structure and the results were considered as good. Sjöstrand states that his model is not sufficient but might be improved by applying SSA on a water domain surrounding the structure. Another approach is to use acoustic elements. This has been studied by Lindgren and Karlsson [11] for an oscillating structure and the result was shown to improve the added mass of a structure submerged in water.

Özarmut [12] uses a similar code to SSA which is Underwater Shock Analysis (USA). Nor does this approach need to generate a mesh for the water in the computational model. It is based on the time dependent differential equations Doubly Asymptotic Approximations (DAAs). USA is said to be most computational efficient and performs such high accuracy that it is worth to use as a complement for ALE and Lagrangian element formulation. This solver requires an additional license which is not available for this master's thesis.

4.3.2 Lagrangian element formulation

Özarmut [12] also studies a method with only Lagrangian elements, where fluid and solid parts of the mesh coincide node to node. The elements in the mesh representing the water have to be refined close to the solid object. This approach can be harder to implement for more complex geometries as the elements between the fluid and solid domains of the mesh have to be connected node to node and can not overlap. A non-uniform mesh in the direction of the shock-wave might have detouring effects on the shock-wave propagation. The study of Özarmut was done for a thin composite panel where no large deformations were expected. This method might thus not be suitable for modelling large deformations and damage.

4.3.3 Arbitrary-Lagrangian-Euler (ALE)

In order to efficiently model a full UNDEX process including the shock-wave propagation, bubble pulses and structural deformations, a solver which handles large deformations and multiple materials is an advantage. This is possible with the ALE solver as the elements can move in space and at the same time allow fluxes over element boundaries. The solver can handle multi-materials within elements with Multi-Material ALE (MMALE). It is then possible to simulate large deformations with domains which contains more than one material. This is especially an advantage when modelling UNDEX, which includes several materials within the fluid domain. ALE can be used together with a structure represented by Lagrangian elements, by implementing a Fluid Structure Interaction (FSI) coupling. In such modelling case, the elements representing the water do not need to be as fine as the Lagrangian elements representing the solid structure. Thus, the mesh of the fluid domain does not need to be connected node to node to the Lagrangian mesh. This is an advantage that will reduce computational cost. [12]

Structured-Arbitrary Lagrangian Euler (S-ALE) is a FE-solver further developed based on ALE. The purpose of S-ALE is to automatically generate a structured computational grid through *keywords*. This is done by defining the geometry of the domain together with element distribution through control points. By doing this, no mesh or domain have to be pre-defined or modelled in a separate file. This can be applied for simple geometries such as rectangular boxes and spheres. Changing the geometry, size and distribution of the mesh will be easier and the solution will be faster as it does not have to import a mesh file. The reason S-ALE is more efficient to compute compared to ordinary ALE is due to the structured computational grid. This allows the solver to pattern the element connectivity and make dependency on data less unpredictable. Therefore the representation of the geometric information can be done by a less extensive database memory. This becomes a big advantage when meshes up towards millions of elements are used. S-ALE uses the same theory to a large extent as the ALE solver and treats multi-materials within elements. [13]

4.4 Fluid Structure Interaction (FSI) and Boundary Element method (BEM)

For a solver to be able to transfer loads between a fluid modelled with ALE elements and a solid modelled with Lagrangian elements, a FSI coupling between these two element formulations is needed. [9]

The FSI coupling tracks and suppresses leakage of fluid into the solid structure. This is done by a penalty-based algorithm that compares fluid penetration relative to the structure's displacement. When penetration is found, node forces are applied forcing the fluid and structure to follow each other. These node forces are proportional to the magnitude of penetration. [14]

Compared to ALE with FSI, the SSA solver uses a Boundary Element Method (BEM). As described earlier, only the structure has to be model. This method includes an iterative process of the DAA which models high and low frequency response asymptotes for a body surrounded by a fluid. A downside with BEM is that cavitation is not accurately captured. A hybrid of FSI and BEM can therefore be performed in order to capture all events during an UNDEX while keeping low computational cost. This can be done by constructing an ALE mesh as a block around the structure and include SSA to initiate the UNDEX. [15]

5 Methodology

The method includes numerical models of different complexities, for solving an UNDEX. This includes modelling the process of an detonation and how it affects a structure. Studies of the structural response are performed in parallel to this, including material and damage modelling as well as natural frequencies. In addition to the use of previous work, experiments are performed in order to compare the numerical approaches. The experiments are described in more detail within this section.

The accuracy of the numerical models is improved during the master's thesis to better correlate with responses from experiments and earlier studies. The process of the work is divided into three main parts, where each part includes a new method for solving an UNDEX in the finite element solver LS-DYNA.

The first part includes modelling an UNDEX with SSA. This simple method of simulating an underwater detonation is compared to more complex models, in order to validate when it can be used as a complement for simple evaluations. It is also compared to analytical calculations and an additional approach for the SSA-model is studied based on earlier work to improve the accuracy.

It is studied whether it is possible to model a fluid domain with S-ALE and still use SSA to initiate an UNDEX. This is included in the second part, where a fluid domain will be constructed surrounding the test object. With this method, physics from the surrounding fluids are included, with the intent of giving more realistic responses.

The third part is to simulate the full process of an UNDEX. This includes everything from detonation, pressure increment, its transfer through the fluid to the object and the structural loads on the object itself. The detonation is initiated and defined by the material *keyword* *HIGH_EXPLOSIVE_BURN, instead of applying a shock-wave with SSA like in the previous parts. The fluid domain is modelled as the experimental set-up with S-ALE. How to treat reflections from the boundaries are also included in this study.

Experiments are executed to compare and calibrate the models. The experiments includes three series with different objectives and are described in detail in Section 5.1. All parts included in the master's thesis are schematically shown in Fig 5.1. Each part is further described in the following sections. The studies of structural responses are carried out in parallel with the fluid modelling methods. These are described within this section as well.

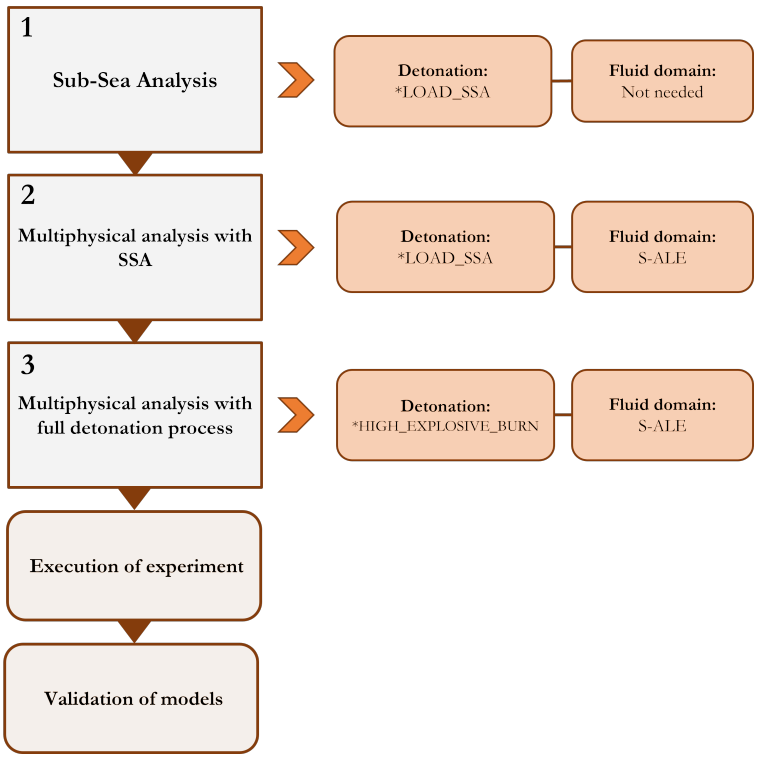

Fig 5.1: View of the methodology for the master's thesis work which includes three parts and experiment before final validation.

5.1 Experiments

Experiments are performed in order to validate the numerical models. The experiments consists of three series with different purposes, these are shown in Tab 5.1. For the first serie, the position of the detonation is gradually moved closer to the cylinder to only receive elastic deformation. For the second serie, where the distance is smaller, plastic deformation is expected. For the third serie, the weight of the explosive material is changed and studied for two positions. This is done in order to see the impact of varying the charge weight instead of distance. Each serie consists of four to five cases for each distance and weight of charge. For the cases where only elastic deformation is expected, the acceleration of the object is also measured. The position of the cylinder is kept constant for all cases, while the position of explosive charge changes.

Tab 5.1: Experimental series.

Series	Variable	Purpose
1	Distance to charge	Low impact with no plastic deformation. Validation for longer distances.
2	Distance to charge	High impact with plastic deformation. Validation of plastic behaviour and bubble pulse.
3	Weight of charge for two distances	Validation of changing weight of charge instead of distance

The experimental set-up is schematically shown in Fig 5.2. The water domain is a 4 m long, 2 m wide and 0.9 m deep pool. The distances from the wall of the domain to the cylinder is 0.85 m. This is to limit interference with the results from reflections. The position of the explosive charge at Case 1:1 is closer to the wall than the test object, because it is more important to limit effects from reflections at the test object.

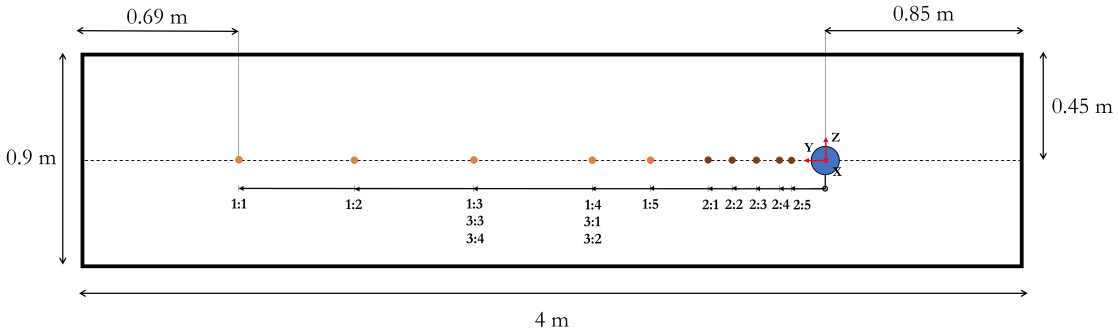

Fig 5.2: Schematic view of experiments. The cylinder is seen within the fluid domain, to the right. The coordinate system is oriented from the center of the cylinder. During Series 1 and 2, the distance is changed while also the weight of charge is changed for Series 3.

The settings for each case are specified in Tab 5.2. The values for the weight of charge are not included due to company confidential restrictions. Case 1:1 and 3:4 were not completed due to the size and lack of strength of the pool encountered when setting up and performing the experiments.

Tab 5.2: Positions of measuring points.

Case	Distance [m]	Weight of charge
1:1	2.50	w1
1:2	2.00	w1
1:3	1.50	w1
1:4	1.00	w1
1:5	0.75	w1
2:1	0.50	w1
2:2	0.40	w1
2:3	0.30	w1
2:4	0.20	w1
2:5	0.15	w1
3:1	1.00	w2
3:2	1.00	w3
3:3	1.50	w4
3:4	1.50	w5

The test object is a cylinder with length 0.3 m, diameter 0.12 m and wall thickness for the pipe of 1.5 mm. The ends have a thickness of 15 mm and are fastened with O-rings, this is to make sure the pipe is deforming and not the ends. The test object is shown in Fig 5.3. The material is Alu 6060 with tensile strength of 140 MPa and fracture strain at 11%. The cylinder is fastened with wires to weights positioned at the bottom of the pool. This is to prevent the cylinder from floating.

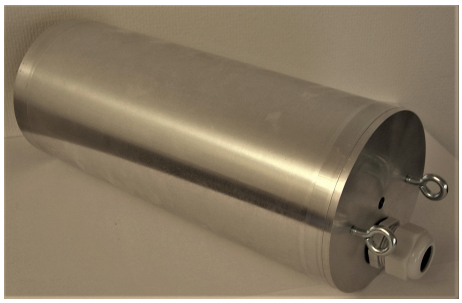

Fig 5.3: Cylindrical test object with cable entity and loops for fastening.

Strain gauges are positioned in the middle part of the cylinder at front, back, top and bottom inside the cylinder, which corresponds to a normal in y, -y, z and -z direction respectively, corresponding to the axis shown in Fig 5.2. They are positioned to measure tangential strains and are shown in Fig 5.4. An accelerometer is positioned at one end, inside the cylinder, and measures acceleration along the y-direction. At the same side, there is a waterproof cable entry.

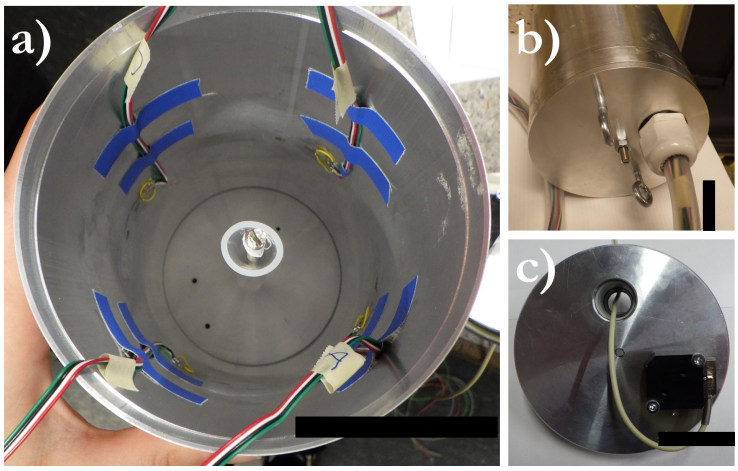

Fig 5.4: The experimental object with the measuring systems attached. a) Strain gauges, b) waterproof cable entry and c) position of accelerometer.

When large deformation is expected (Case 2:5), no measuring system was attached to the cylinder and only the visual plastic deformation was studied. A pressure gauge was positioned in the water to validate the analytical equations and the S-ALE solver. The experimental set-up is shown in Fig 5.5, where the water domain can be seen, the cylinder positioned in it, the position of the charge and pressure gauge for Case 2:1.

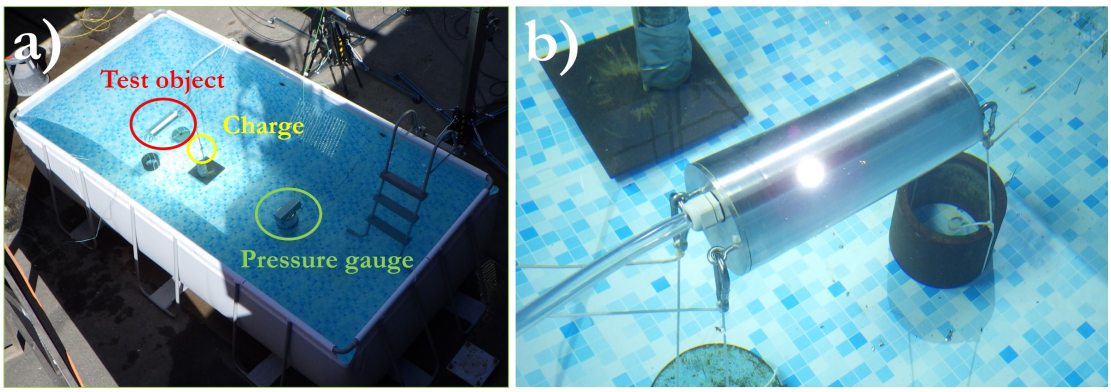

Fig 5.5: a) Set-up of the pool where test object, charge and pressure gauge is positioned, b) Test object positioned and fastened.

5.2 Earlier work for validation

During the validation of models and methods, not only the experiments are used for comparison. Earlier work is used to compare responses with SSA. The first reference work is experiments executed by De Candia et al. [15]. The experimental object was a 12 m long pipe with diameter 0.4 m and a wall thickness of 6.35 mm. The cylinder was of C350 grade cold-rolled steel and 250 g of Pentolite was detonated 1.8 m from the center of the cylinder. Additional weights of 225 kg were applied in the experiment at each end of the cylinder. This was included in the numerical model by increasing the density of the material at the ends. Strain responses on specific positions of the structure were measured during their experiments and can thereby be compared to the results in this master's thesis. A schematic top view of the cylinder is shown in Fig 5.6. For more details about the experiment, see [15].

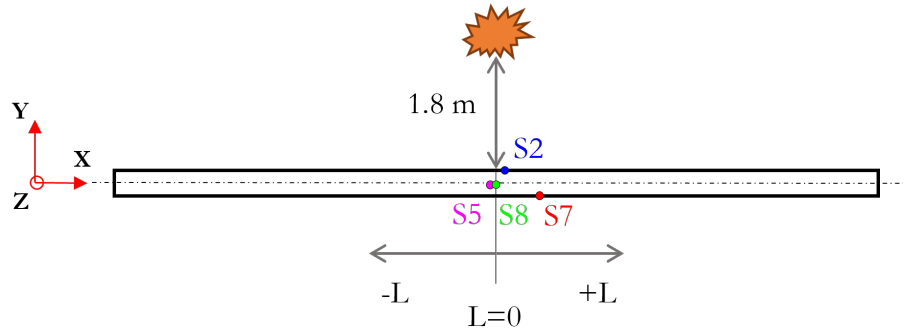

Fig 5.6: Schematic view of experimental cylinder from earlier work and measuring points.

The measuring points have a small variation of axial position and are therefore specified in Tab 5.3. As seen from Fig 5.6, the distance is measured from the center of the cylinder. All positions measures axial strain.

Tab 5.3: Positions of measuring points.

Position label	L [mm]
S2	75
S5	-50
S7	300
S8	0

The model of the cylinder was built with shell elements and was assumed to be sufficiently fine for the studies it is used for. This assumption was based on that an extensive resolved mesh could be applied due to the low computational cost of the study. No mesh convergence study was made for this model as it was not a major part of the work. Elastic material with parameters from the earlier work is used and the model is shown in Fig 5.7.

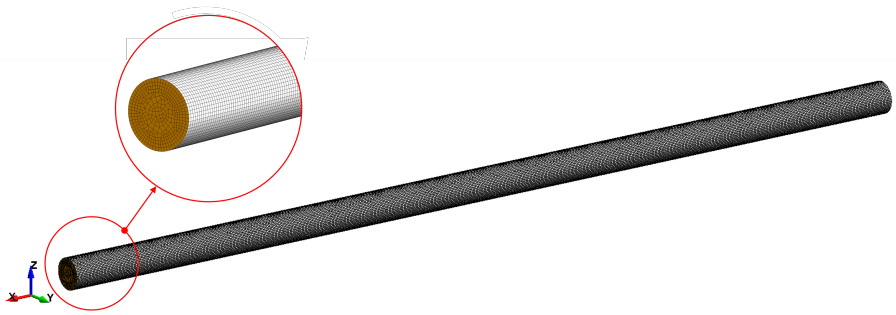

Fig 5.7: Numerical model of the cylinder from [15].

The second experiment is from a study of Monterrubio and Krysl [16]. They studied natural frequencies in water for five different geometries, and the first unconstrained cylinder is the one used for this study. Their experimental data is used for comparison. The cylinder is 1.284 m long with a diameter of 0.357 m. The wall thickness of the pipe and ends are 3 mm. The density of the material is 7750 kg/m^3. The same arguments for the chosen mesh mentioned above, applies for this model as well. An elastic material model is used and the meshed model is shown in Fig 5.8.

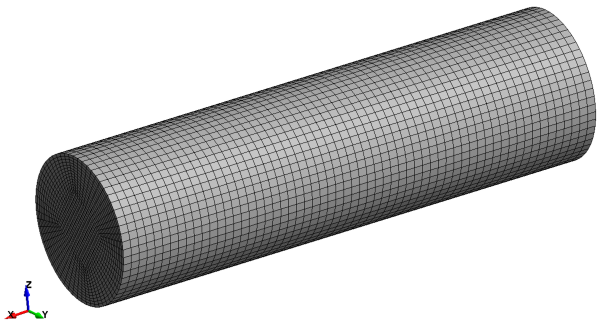

Fig 5.8: Numerical model of the cylinder from [16].

5.3 Numerical model of test object

The test object is modelled as a closed cylinder with thicker ends with dimensions as the test object. Shell elements are used with the formulation ELFORM=-16, which is fully integrated shell elements modified for higher accuracy. The simulation is run with an explicit solver where timestep is set automatically. The material model *MAT_24 is used to define material properties and to be able to receive plastic behaviour.

The cylindrical model is shown in Fig 5.9 and is used for all simulations of the experiments. To the right, it is shown where the front, back, top and bottom is positioned in relation to the global coordinate system. It is not constrained in any translational or rotational direction when modelling with SSA, thus the cylinder will be treated as neutrally submerged free in water. When using S-ALE, the cylinder is constrained in z-direction to prevent it from floating. A mesh with 8174 elements was studied and compared with a finer mesh of 13784 elements. The peak strain value, for Case 1:5, differed with 8×10^{-6} and the finer mesh was further chosen to ensure high accuracy for all studied cases and to work well for the FSI coupling with S-ALE.

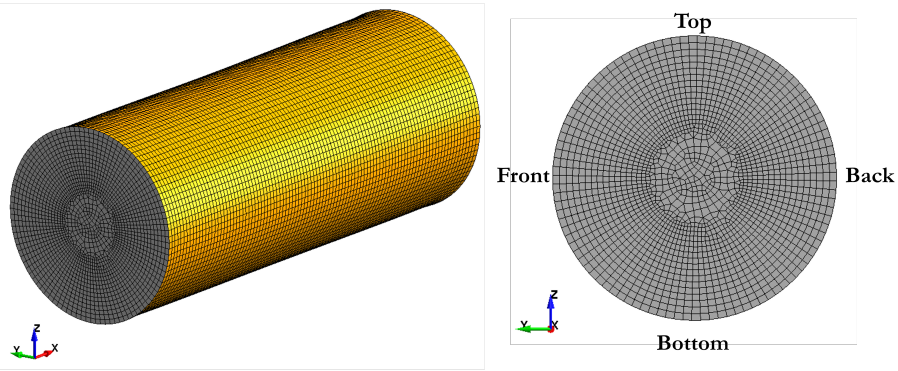

Fig 5.9: The meshed model of the cylinder for the experiments.

5.4 Sub-Sea Analysis (SSA)

The aim of this part is to validate this method, compare it to analytical calculations and later also other the modelling methods and experiments. From this study, it should be concluded within which specification area of UNDEX cases this simplified model can be used. This includes parameters such as distance to detonation and weight of the explosive material. It is possible to account for sea floor reflections with SSA, and this will be used when simulating the experiments. A flooding status has to be defined in the *keyword* *LOAD_SSA where the setting for air inside and fluid outside is used for the cylinder. This means that pressure will only be applied on the outside of the cylinder. For the speed of sound in water the value 1500 m/s is used.

The SSA model is compared to analytical calculations where it should be found at which distance the results correlate. Eq (2.1),(2.2),(2.3) and (3.1) are used for analytical calculations.

It has been found in earlier work that a layer of water elements can improve the accuracy of SSA [7]. The experiment cylinder is used together with a box surrounding it. The mesh consists of tetrahedral acoustic elements, with element size of 10 mm at the boundaries. This approach by using acoustic elements was earlier studied by Lindgren and Karlsson [11]. A view of the mesh is shown in Fig 5.10 with a) the cylinder positioned inside and b) a section view of the solid tetrahedral mesh. The material model is developed for low pressure stress waves and cavitation can optionally be allowed [9].

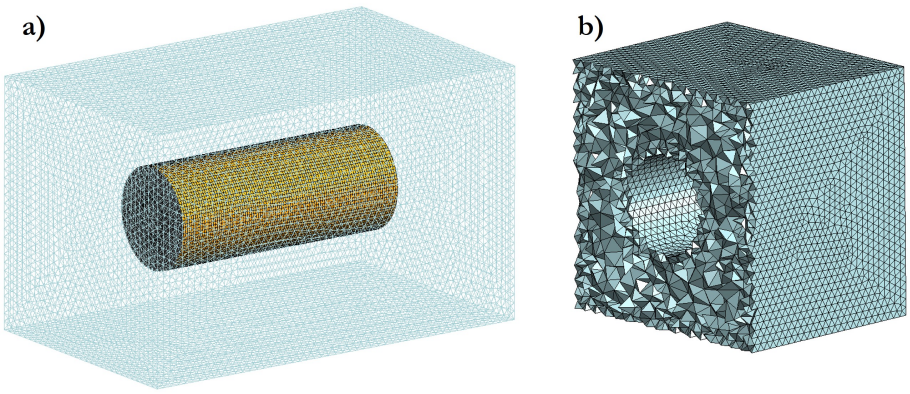

Fig 5.10: a) Mesh of box with cylinder inside and b) section view of solid tetrahedral mesh.

5.5 Multi-physical analysis with S-ALE

The multi-physics analysis includes both water, air and the test object. It is performed using a S-ALE mesh that is generated with the use of control-points. These control points prescribe the dimensions of the S-ALE mesh domain in x-, y- and z-direction, as well as the distribution of elements in these directions. A full scale model of the experiments is created as well as a smaller water domain for a further implementation of SSA.

For both models, the S-ALE mesh inside the cylinder is filled with air at atmospheric pressure level. The air follows the Linear Polynomial EOS while the water follows the Gruineisen EOS. To prevent the cylinder from floating, two nodes on the ends are locked in z-direction. This is a similar constraint to what will be used for the experiments when the cylinder is tied to the bottom using wires. The coupling between the S-ALE mesh and the shell mesh of the cylinder is performed with the use of FSI couplings.

Along all boundaries of the S-ALE domain the first layer of elements have been given the characteristics to represent an ambient open boundary. This boundary condition (BC) is intended to make the simulation representing a portion of fluid taken from a large domain of water, like the open sea with the aim of avoiding reflections of the shock-wave from domain boundaries. Hydrostatic conditions are applied to the water filled part of the S-ALE mesh, so in turn the cylinder is exerted to a pressure equal to being submerged in water.

With the introduction of S-ALE, LS-DYNA has also introduced *keywords* more suited for S-ALE that are intended to be easier to implement. Below in Tab 5.4 can the old ALE *keywords* and the new corresponding for S-ALE be seen.

Tab 5.4: *Keywords* for ALE and their corresponding S-ALE version.

ALE *keywords*	S-ALE *keywords*
*ALE_MULTI-MATERIAL_GROUP	*ALE_STRUCTURED_MULTI-MATERIAL_GROUP
*INITIAL_VOLUME_FRACTION_GEOMETRY	*ALE_STRUCTURED_MESH_VOLUME_FILLING
*CONSTRAINED_LAGRANGIAN_IN_SOLID	*ALE_STRUCTURED_FSI

The aim was at first to implement S-ALE together with all these new *keywords* for these simulation models. A lot of time and effort was put into the model in order for it to work properly, scaled down models were therefore created. However, these downsized models were very hard to get stable, mainly when it comes to the pressure distribution and FSI coupling.

It was found that the down-scaled models with the old ALE *keywords* tended to be more stable than when using the S-ALE *keywords*. Sjöstrand [7] used the old ALE *keywords* and obtained sufficient results. Because of this, the older ALE *keywords* were used when creating the studied models. The mesh was, however, of S-ALE elements instead of ordinary ALE elements.

5.5.1 Multi-physical analysis with SSA

As mentioned earlier, SSA can become more accurate by modelling fluid elements surrounding the structure. This is done together with a S-ALE domain which contains water surrounding the cylinder and air on the inside of the cylinder. This S-ALE domain has the dimensions $0.8\times0.5\times0.5$ m. The domain was intended to have same dimensions as the one for acoustic elements, but with that size the BCs did make the pressure in the domain unstable, so it was enlarged. The S-ALE mesh can be seen in Fig 5.11 with the cylinder located in the middle.

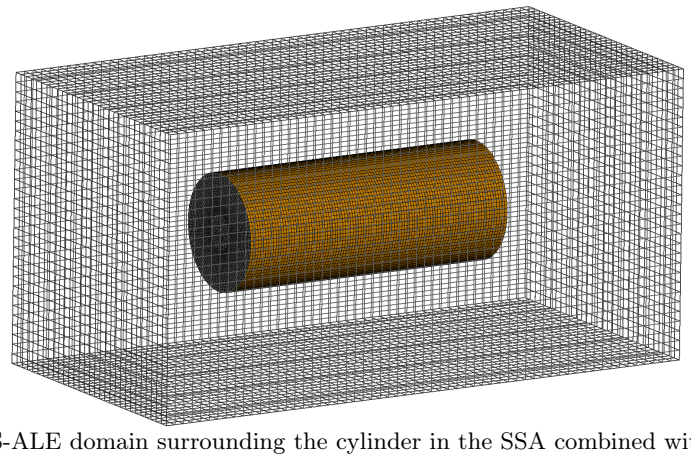

Fig 5.11: The S-ALE domain surrounding the cylinder in the SSA combined with S-ALE model.

Like in Section 5.4 SSA was used to initiate the detonation. The detonation point is outside the S-ALE domain and SSA is applied on the cylindrical test object. This is done because applying SSA on a S-ALE mesh was not possible. As found by Nawa and Just [10], this surrounding water can improve the result compared to only using SSA because the added fluid includes more physics. This can assist the global structural responses of the whole cylinder, such as acceleration levels and oscillations due to natural frequencies.

5.5.2 Multi-physical analysis with full detonation process

This S-ALE domain is filled using three multi-material groups: explosive, water and air. The computational domain is filled in several steps. Firstly, the explosive material is put in the domain and then water fills everything around it. After that, the parts of the domain inside the cylinder and above z=0.45 m are filled with air.

The detonation is initialised using *INITAL_DETONATION. This *keyword* is coupled to a multi-material group and the JWL EOS that defines the explosive material. Below in Fig 5.12, a section through the YZ plane can be seen, showing how the domain is filled with the different materials.

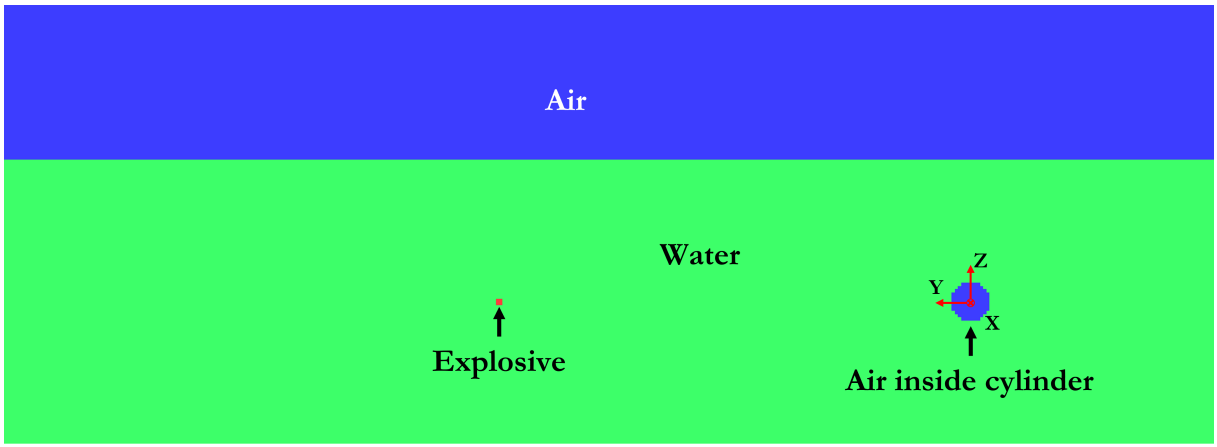

Fig 5.12: Schematic view of how the multi-material groups are divided in parts of the S-ALE domain.

5.5.3 Mesh verification S-ALE

For the main S-ALE model that represents the experimental domain, a mesh verification is performed. For this, it is assumed that the Lagrangian mesh for the cylinder is resolved enough from the implementation of the SSA model. So only the resolution of the S-ALE mesh is altered during this verification.

The mesh is constructed in such a way that the most refined region is where the primary shockwave and bubble pulses will transmit from the detonation to the cylindrical test object. The cell size in this region is the control parameter that is altered. Outside this region a growth ratio of 1.1 [17] is applied to allow for a reduced cell count while not having any significant impact on the results. Below in Fig 5.13 and 5.14 it can be seen how the mesh refinement is distributed in relation to the position of the explosive material and cylinder. The YZ-plane is displayed in Fig 5.13. The refined region is extended in y-direction long enough to be able to include both the cylinder and the explosive material when the detonation point is the furthest away from the cylinder.

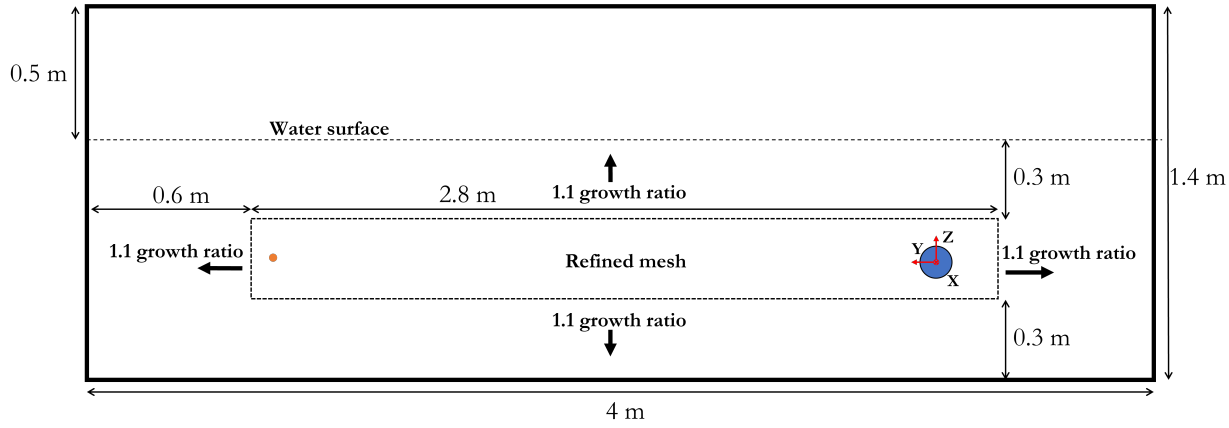

Fig 5.13: Schematic view of where the region that is targeted in the refinement is located in the YZ-plane of the computational domain. This is an illustration when the explosive material is located furthest away from the cylinder.

The XZ-plane of the refined domain is shown below in Fig 5.14. This shows how the refined region extends 0.3 m on each side of the cylinder in x-direction. In z-direction, the refined region has a height of 0.3 m, roughly three times the cylinder diameter and is centered around the cylinder.

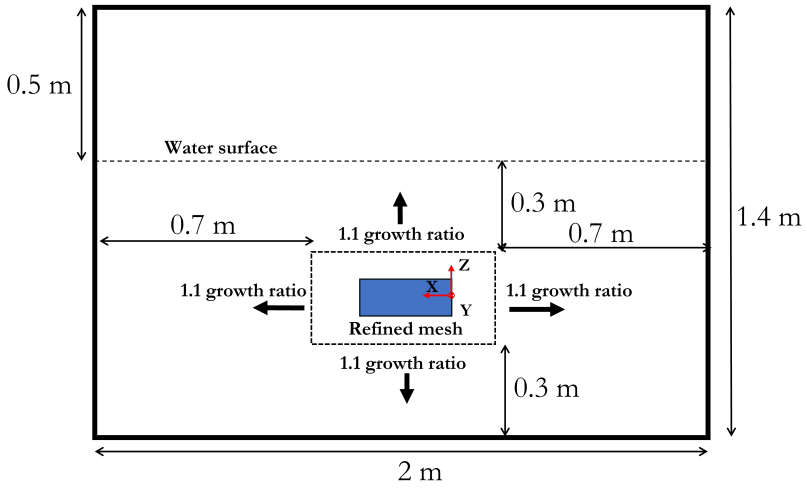

Fig 5.14: Schematic view of where the region that is targeted in the refinement is located in the XZ-plane of the computational domain.

In the refined region, the cell size is always equal in all directions, and hexahedral elements are used. Outside of this region, the elements grow according to the set growth ratio, which is set to 1.1 in all directions. During the mesh verification four different meshes are compared. Statistics from respective mesh can be seen in Tab 5.5.

Tab 5.5: Parameters and statistics from mesh verification.

Mesh	Cell size	Refinement factor	Number of elements	Number of elements increase
Coarse	2 cm	-	453 596	-
Medium	1.5 cm	0.75	898 778	98%
Fine	1 cm	0.66	2 270 520	153%
VeryFine	0.75 cm	0.75	4 724 883	108%

The selection of cell sizes were based on the previous work by Sjöstrand [7], where he had a ratio between diameter of explosive material and cell size at 1.32. Meaning the diameter of the explosive material was 1.32 times larger the cell size at the detonation point. Applying this on our explosive charge gives a cell size of 1.5 cm, this cell size is therefore used for the first examined mesh, cell sizes both larger and smaller than this are also examined. However, according to personal communication with Dynamore Nordic AB, the ratio between explosive charge diameter and mesh size need to be around 10 to properly resolve the UNDEX. This would in turn give a cell size close to 0.2 cm which leads to computationally challenging simulations and is, therefore, not applied. This will be taken into consideration during the evaluation of the mesh verification.

The studied parameters in this mesh verification are pressure at two points in the S-ALE mesh together with the tangential stress at two points on the cylinder's Lagrangian mesh. Pressure in the S-ALE mesh indicates how well the S-ALE mesh resolves the detonation and propagation of the shock-wave. The tangential stress in the cylinder indicates how well the S-ALE transfers the load from the shock-wave onto the cylinder through the FSI coupling.

The pressure at two points in the S-ALE mesh is studied and presented in Fig 5.15 for all meshes, 100 mm in front and to the side of the cylinder respectively. It can be seen that the pressure for the coarse mesh does not change from the initial hydrostatic pressure. This indicates that this mesh is too coarse to resolve any of the detonation and shock-wave propagation. All the other meshes have similar pattern of oscillative responses but with different magnitudes. The offset between the medium and fine mesh is rather large and some peaks are not resolved for the medium mesh. The alignment between the fine and very fine mesh is better, both in terms of offset in the magnitude and the resolved peaks.

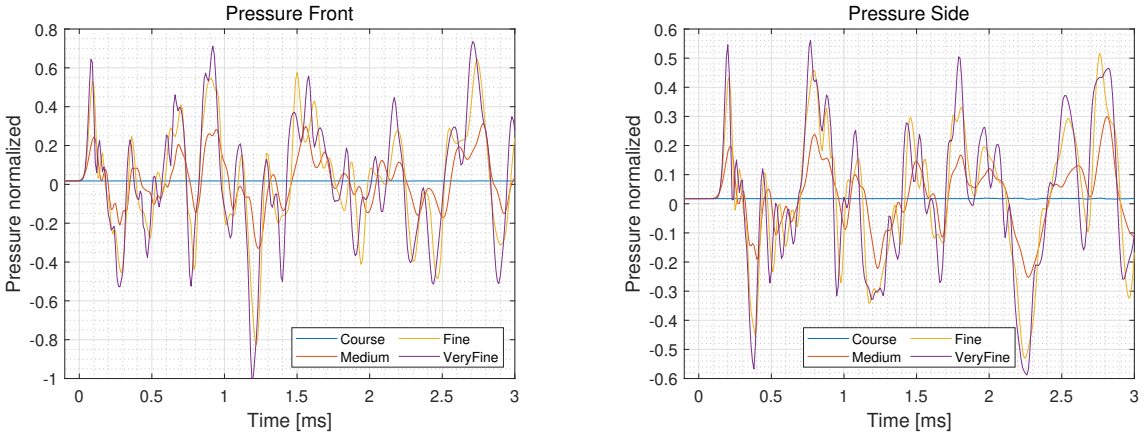

(a) **(b)**

Fig 5.15: Pressure at two points in the S-ALE mesh, a) 100 mm in front of the cylinder and b) 100 mm to the side of the cylinder. t=0 is when the shock-wave reaches the point in front of the cylinder.

Below in Fig 5.16 can it be seen how the tangential stress at the top and back of the cylinder varies for the different meshes. In the same way as for the pressure, the behaviour of the stress is oscillative. For both, this can be due to reflections from the boundaries in computational domain. In addition the oscillations of the stress can also be contributed by shock-waves hitting the cylinder and matching its natural frequencies. The coarse mesh does not show any significant stress, likely due to the badly resolved detonation and shock-wave that was discovered in Fig 5.15. The alignment between the fine and very fine meshes are good compared to the alignment between the medium and fine meshes, especially for the first two peaks. There are large discrepancies between the fine and very fine meshes, however. This is believed to be a consequence of a combination of reflections and natural frequencies that respective mesh resolves or triggers differently.

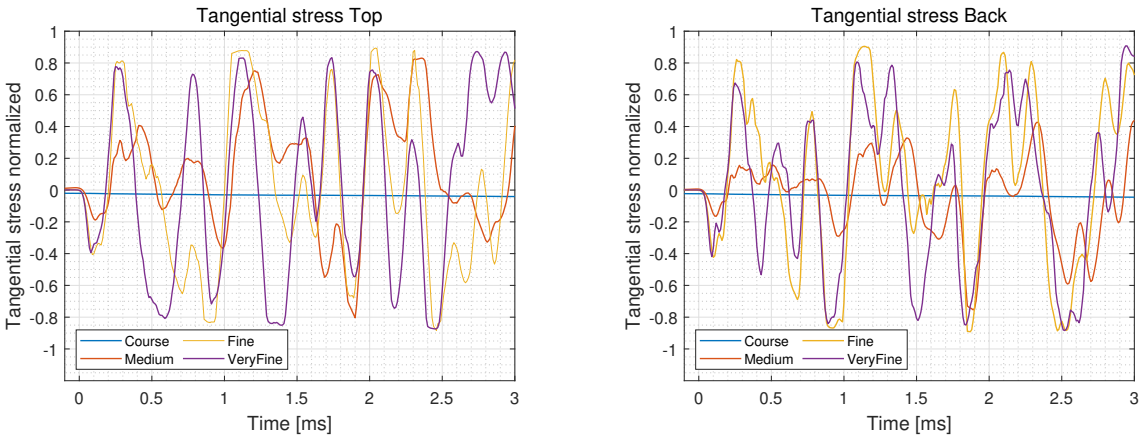

(a) **(b)**

Fig 5.16: Tangential stress at the top (a) and back (b) of the cylinder for respective mesh. t=0 is when the shock-wave reaches the cylinder.

The alignment between the fine and very fine mesh is rather good, especially in the beginning when the shock-wave hits the cylinder. Further into the simulation, the alignment is not as good, indicating that reflections are not resolved and natural frequencies are not triggered as good as for the primary shock-wave. The computational load was also found to be significantly higher for the very fine mesh. Due to limited computational resources and time, the fine mesh is deemed to be good enough and will from here on be used for all S-ALE simulations. This gives a ratio between explosive charge diameter and cell size around 2, which is not as good as the recommended 10 from Dynamore Nordic AB, but it is good enough to resolve the initial shock-wave.

5.6 S-ALE performance

In this section some evaluation of the S-ALE model's performance and initial results are carried out. Focusing on how the model behaves compared to what is expected and desired.

In the setup of the S-ALE model, BCs were applied to remove the effect from reflections in the boundaries of the computational domain, as explained in Section 5.5. However, during the mesh verification when the shock-wave behaviour also was examined, it was found that the shock-waves did reflect in the domain boundaries. An additional simulation was performed where the nodes at the boundaries of the domain were no longer locked. Below in Fig 5.17 a comparison can be seen of how the shock-wave pressure behaves for both cases. In the center is the detonation point that the shock-wave propagates from and to the sides can the shock-wave propagation be seen. Above the detonation point can a reflected shock-wave be seen, this is a surface reflection that should occur. Below the detonation point can a similar reflection be seen from the bottom of the domain that should not occur. It can therefore be stated that locking the nodes along the domain boundaries seems to have no effect on how the shock-wave reflects in the boundaries. Also it can be stated that the ambient BC does not work as intended, letting the shock-waves continue out of the computational domain and avoiding reflections.

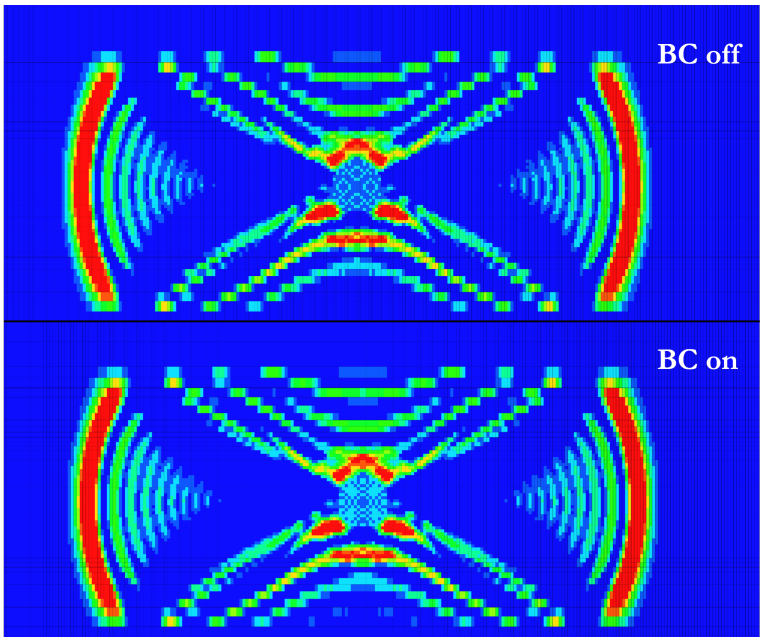

Fig 5.17: Reflections from domain boundaries for cases where nodes at domain boundaries are locked (BC on) and free (BC off).

The reason for reflections occurring despite using ambient BC can be that this BC prescribes a certain hydrostatic pressure that should be upheld at the domain boundaries. When the high pressure shock-wave then reaches these boundaries this prescribed pressure does act as a type of wall or change in fluid properties. This can be why similar reflections are seen from the water surface and bottom. When in reality they should behave differently, one being a tensile and the other being a compressive shock-wave.

As there is no clear alternative approach to removing the effects from reflections in the domain boundaries, the ambient BC is kept with the same locked nodes along all boundaries. This is also due to the limited time of this master's thesis. Considerations for how these reflection affects the results will have to be taken.

5.7 Natural frequencies

When the bubble is expanding and collapsing, the frequency of the pulses may coincide with a natural frequency of a structure. This can damage certain components or a whole structure. This can also be triggered by the primary shock-wave. The behaviour of a structure depends on the surrounding fluid, which is why the natural frequencies in water differs from air. To calculate the natural frequencies for a structure submerged in water, the added mass method is used.

In order to study this behaviour of natural frequencies, two earlier work presented in Section 5.2 are compared with, since they both have result of natural frequencies in water. The density of the material is increased until the result correlates with the studies.

The first study is with the cylinder from De Candia et al. [15]. The density of the pipe, not the ends, is increased until the results correlated with the experiment. They calculated the natural frequencies by using the USA code, which was shortly explained in Section 4.3.1. For the second cylinder from Monterrubio and Krysl [16], the density of both the pipe and ends are increased, since they have the same thickness initially.

6 Results and Discussion

A variety of modelling methods and geometries are studied and the results are presented and discussed within this section. SSA is compared with analytical calculations, pressure responses from S-ALE are compared to experiments and analytical calculations. Further are some of the experimental cases brought up and discussed. The pressure results are normalised for all cases. Due to the heavy computation with S-ALE, not all cases are simulated. Therefore, some cases are only compared to SSA, which is more time efficient. Positive values of strain is defined as tensile strain for all cases except for the analytical validation in Section 6.1.

6.1 Analytical validation

The SSA method was validated with analytical calculations from Eq (**??**) and (3.1). The numerical model of the test object was used for the simulations and the detonation is initiated after 1 ms. The maximum stress caused by the primary shock-wave decreases as the detonation is initialised at a longer distance away from the cylinder. This is shown in Fig 6.1, where distances from 2 m up to 50 m was evaluated for compressive tangential stress at the front. Comparing simulated result to analytical, it was found that the difference decreases for longer distances. For the first case at 2 m, the analytical result is 65 MPa. To be able to visualize and present the rest of the results in a good way, the analytical value for 2 m is not shown within the graph. The offset decreases as the distance increases, thus it is more critical to model a detonation close to a structure where the impact is more local and cannot be simplified as an evenly distributed pressure load.

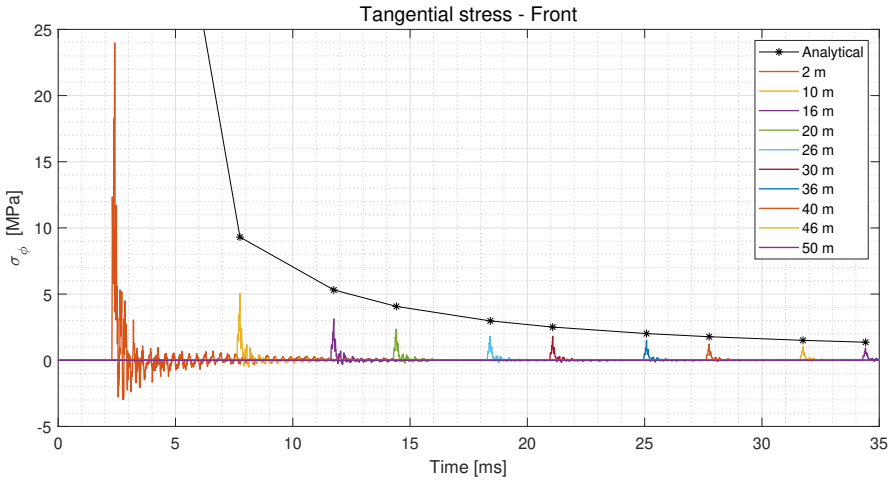

Fig 6.1: Tangential stress response at the front of the cylinder when varying distance to detonation. Analytical result is included for comparison.

6.2 Natural frequencies

Natural frequencies of structures submerged in water are studied. The first study is done for the 12 m long cylinder used by De Candia [15]. Results for the natural frequencies are presented in Tab 6.1 and it shows dry and wet values when increasing the density to correlate with the source listed in the table. An increase of around 20 000 kg/m^3 is needed in order to find correlating results, this correspond to a weight of 1600 kg. It is also noted that for lower frequencies, higher density need to be used.

Tab 6.1: Comparing wet natural frequencies from [15] with the added mass method. An increment of the density results in better correlation with wet values.

	Added density [kg/m^3]				
De Candia [15]	0 (Dry)	17170	19170	22170	27170
6.8 Hz	11.1 Hz	7.7 Hz	7.5 Hz	7.2 Hz	6.9 Hz
20.3 Hz	35.0 Hz	22.0 Hz	21.4 Hz	20.6 Hz	19.3 Hz
41.6 Hz	72.7 Hz	43.0 Hz	42.5 Hz	40.7 Hz	38.1 Hz

The result for the second cylinder is shown in Tab 6.2. Similar behaviour is found here, more mass has to be added for lower frequency levels. It can be because of the mode motion where lower natural frequencies has larger oscillations, thus contributes to more displaced fluid.

Tab 6.2: Comparing results to second studied cylinder. An increment of the density results in better correlation with wet values.

	Added density [kg/m^3]				
Monterrubio and Krysl [16]	0 (Dry)	12250	17250	19250	22250
96 Hz	196 Hz	122 Hz	109 Hz	105 Hz	99 Hz
107 Hz	205 Hz	128 Hz	114 Hz	110 Hz	104 Hz
199 Hz	359 Hz	223 Hz	200 Hz	192 Hz	182 Hz
214 Hz	391 Hz	243 Hz	217 Hz	209 Hz	198 Hz
239 Hz	418 Hz	260 Hz	233 Hz	224 Hz	212 Hz

To further study the behaviour of SSA, natural frequencies are extracted at certain timesteps during a simulation. This is done to see if SSA takes the damping effects of water into account. The *keywords* *CONTROL_IMPLICIT_EIGENVALUE and *CONTROL_IMPLICIT_GENERAL are used and a curve is defined that samples eigenvalues during the simulation, before the detonation was initiated. This is done for both cylinders, and the result is compiled in Tab 6.3. The result is the same as for the dry results above. This indicates that SSA does not account for the water when it comes to frequency studies. De Candia [15] used the USA code to simulate the responses and also to find the natural frequencies in water. A difference between USA and SSA is thereby found, where USA includes the physics of water in a more appropriate way during frequency studies.

Tab 6.3: Natural frequencies for both cylinders when simulating with SSA.

De Candia [15] cylinder with SSA	Monterrubio and Krysl [16] cylinder with SSA
11.1 Hz	196 Hz
35.0 Hz	205 Hz
72.7 Hz	359 Hz
-	391 Hz
-	418 Hz

The manual for LS-DYNA [9] says that SSA accounts for the primary shock-wave and the bubble pulses. To study this further, a longer simulation to capture the bubble pulse is performed. It is studied whether the bubble pulse can trigger the first mode, which would lead to oscillations of the structure. De Candia's cylinder is used to simulate the bubble pulse and the result is compared to Figure 19 in [15]. The previous result showed that SSA did not give the right frequencies with the correct material density, this is therefore also studied with increased density

corresponding to the first mode at 6.9 Hz.

It is found that only the effects from the first bubble pulse is received with SSA, this can be seen in Fig 6.2. The period time for the pulsation is approximately 150 ms, corresponding to a frequency of 6.7 Hz, which is close to the lowest natural frequency. De Candia [15] finds oscillating responses during experiments but the mode is not triggered with SSA even if the density is increased. The result for increased density captures the bubble pulse similarly as for a dry cylinder. Because of increased density, the speed of sound for the material increases. The effects from this can be seen in the result for the case with increased density, where the shock-wave responses reaches higher levels.

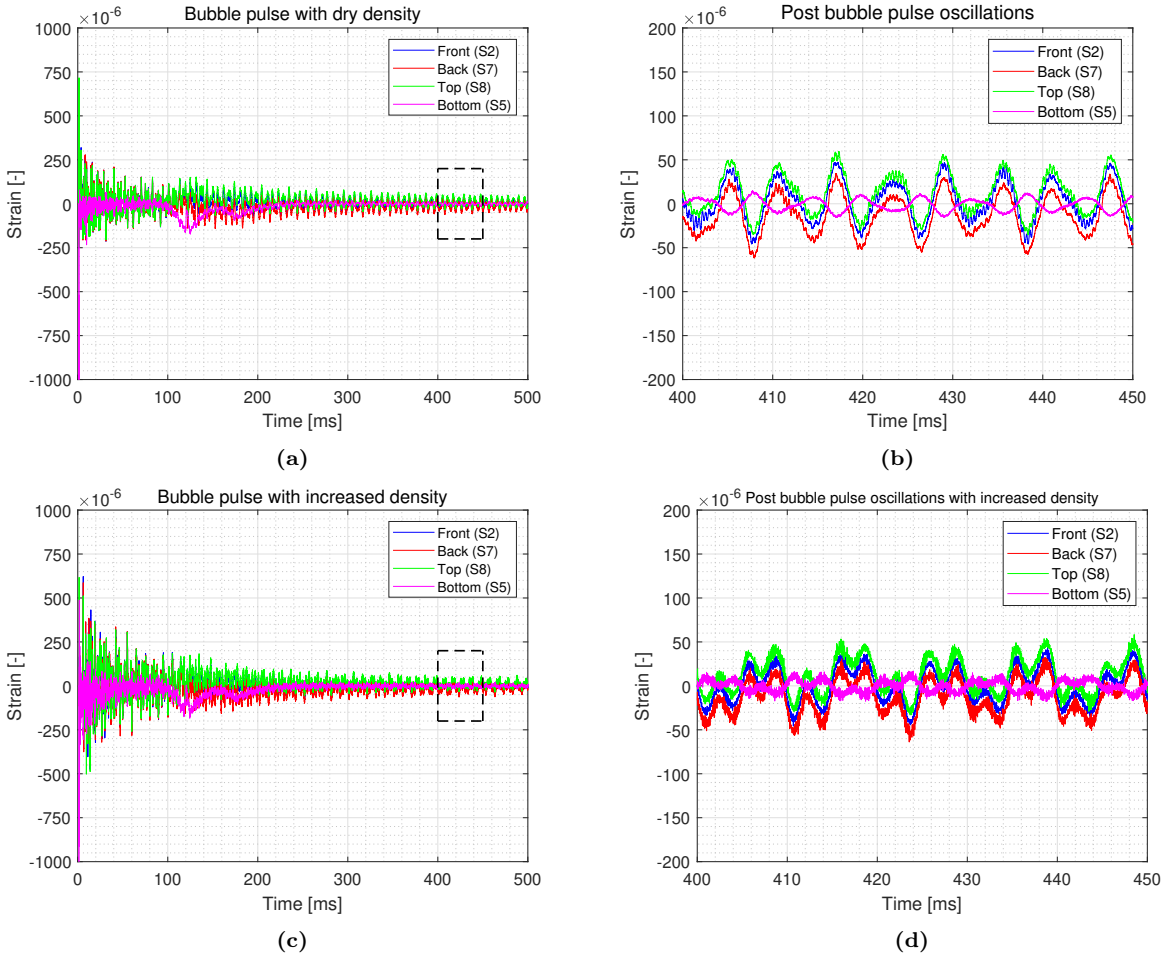

Fig 6.2: Bubble pulse simulation with (a) dry density and (c) increased density. A zoomed in view is shown for (b) dry density and (d) increased density.

When increasing the density, there are high frequent oscillations which is not found for dry density. It is difficult to point out one specific reason, but when increasing the density, the behaviour of the structure changes and it may disturb the structure in more ways than intended. The shape of the oscillations after the bubble pulse differs slightly and the frequency of the oscillations has a small deviation, but the overall behaviour between the measuring points remains for dry and wet condition. The bubble pulse is mostly represented in the response from the element positioned at the bottom of the cylinder. The reason for this can be due the positions of the measuring points which do not align axially due to the experimental set-up from De Candia [15]. The modelled cylinder does also have deviations from the experiment which can contribute to errors in the result. In order to replicate the experiment more accuratly, the whole test rig should be modelled. It would also be interesting to study a way of applying weight onto the

model without changing the density of the material. Some things can still be pointed out from this. Natural frequencies can not be triggered in SSA by modifying the model with the added mass method. It should be further studied what triggers the oscillations found in the result, it could be from the primary shock-wave or only due to the bubble pulse.

6.3 Experiments

The results from the experiments consist of strain and acceleration measures for some cases and pressure levels at a certain distance from the detonation point. For the critical cases when extensive plastic deformation was received, only visible deformation was studied. The most important findings from the experiments are presented and compared to other models. During the experiments, some strain gauges were damaged and therefore not all positions are presented in the results.

6.3.1 Pressure validation for analytical calculations and S-ALE

Firstly, the pressure at a certain distance from the detonation was measured by four different distances during the experiments. The pressure can also be calculated analytically by Eq (**??**) or received from the simulations with a S-ALE domain. The peak value from the primary shock-wave is studied. The pressure sensor was not always positioned at the same distance from the explosive charge as the cylinder. Therefore only the distance R is presented and not the specific case. The values from analytical calculations, experiments and S-ALE are presented in Tab 6.4. The values are normalised with the experimental result for each distance due to a variety for the weight of charge, therefore it is presented as equal to 1. Overall, it can be observed that the experiments gave higher pressure responses and S-ALE lower than the analytical values. S-ALE performs best for the case with a distance of 1.5 m, this is likely due to the explosive charge having a more favorable size relative to the mesh cell size. Therefore giving a better resolved primary shock-wave. The accuracy for S-ALE responses increases for larger distances, indicating that the shock-wave pressure decay is slower for S-ALE compared to the analytical expression. This can become problematic for better resolved shock-waves that occur further away. The analytical result is closer to the experiments, for both shorter and longer distances. The largest difference is when S-ALE performs best, at 1.5 m. Similarly as the weight of charge was more advantageous for S-ALE, it decreased the accuracy of the analytical calculations.

Tab 6.4: Peak pressure values from experiments, analytical calculations and S-ALE.

Distance (R) [m]	Experiments	Analytical	S-ALE
2	1	0.94	0.25
1.5	1	0.55	0.35
1.35	1	0.80	0.19
0.75	1	0.99	0.13

In Fig 6.3 can the normalized pressure be seen for the experimental and analytical results at the distance of 0.75 m, S-ALE result is not included in the graph as it differed a lot. It can be seen that the peak values correspond well and also the slope of the pressure decay until the pressure decreases to approximately 30% of its peak value. This is to be expected as the analytical pressure expression (Eq. (**??**)) is only accurate until the pressure has decreased to 37% of its peak value [1]. Some disturbance response is seen around 0.3 ms in the experimental results. This is likely to come from reflected shock-waves.

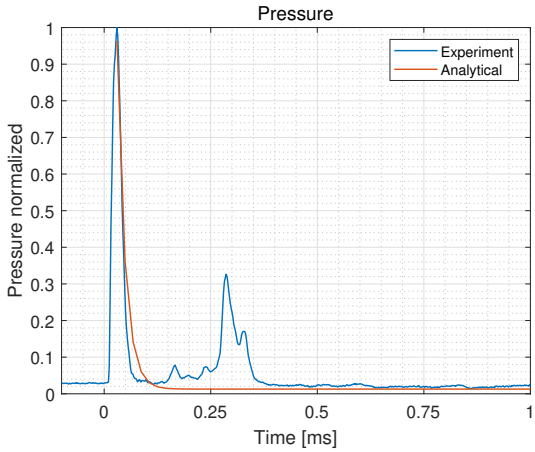

Fig 6.3: Normalized pressure for the experiments and analytical solution for 0.75 m distance to the UNDEX.

6.3.2 Strain response for Case 1:3

For Case 1:3, the distance was 1.5 m. The result for the strain response at the top, back and bottom of the cylinder is seen in Fig 6.4 together with result for the same case with SSA. The simulated result shows an ideal case where the shock-wave gives high responses and the first bubble pulse correlates quite well with the analytical calculations, which gives a bubble pulse after 43 ms. Because of extremely high peak responses from the shock-wave with SSA, it is not included in the graph. The maximum strain response for SSA reaches -900$\times 10^{-6}$. The experimental results differ from the simulated. A response is found when the shock-wave arrives, but not as high magnitudes are reached as for SSA. The magnitude of the experimental strain response at the shock-wave is in level with the bubble pulse response for SSA.

There are multiple factors that impacts the experimental result leading to differences compared to SSA. No reflection responses are found with SSA, but it is expected that the cylinder during the experiments is exposed to reflections from bottom and sides of the pool as well as the water surface. For the experiment, the strain gauge at the top of the cylinder reaches higher strain at the same time when the bubble pulse is initiated in SSA. This could therefore be a response of the bubble pulse even though it is not as distinct as for SSA. There is also a change in behaviour at around 70 ms. Due to the irregular oscillations following after that, this is considered as disturbances from reflections.

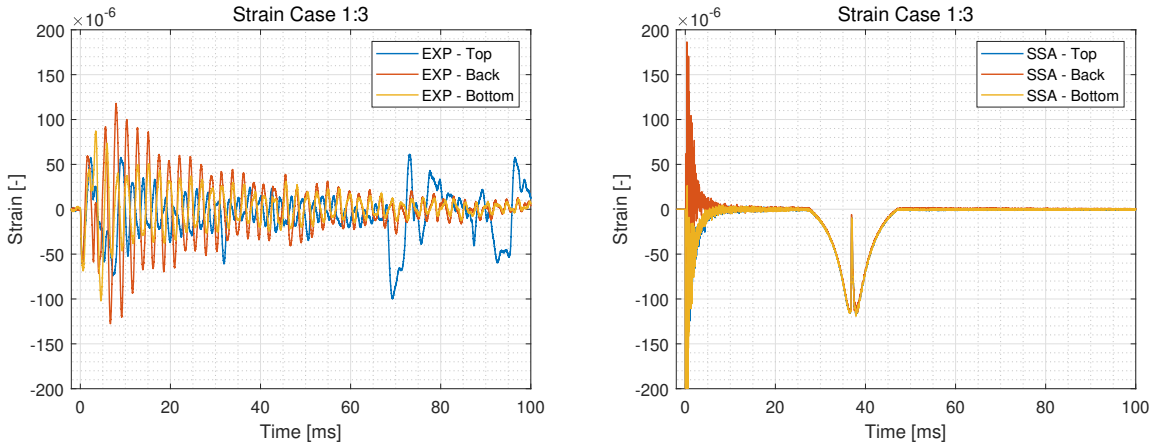

Fig 6.4: Result of strain from Case 1:3 for a) experiments and b) SSA model.

6.3.3 Strain comparison of Case 1:4 and 3:2

Case 1:4 and 3:2 are compared because the distance to the charge is the same, but the weight of charge differs. It is found from Fig 6.5 that the magnitude of strain increases for a larger weight of charge. The result for the top of the cylinder is presented. Except for the peak value, the responses in SSA are lower than for the experiments. It is once again seen that SSA gives oscillations of a higher frequency. To further investigate this behaviour, a frequency study was done for the experimental cylinder.

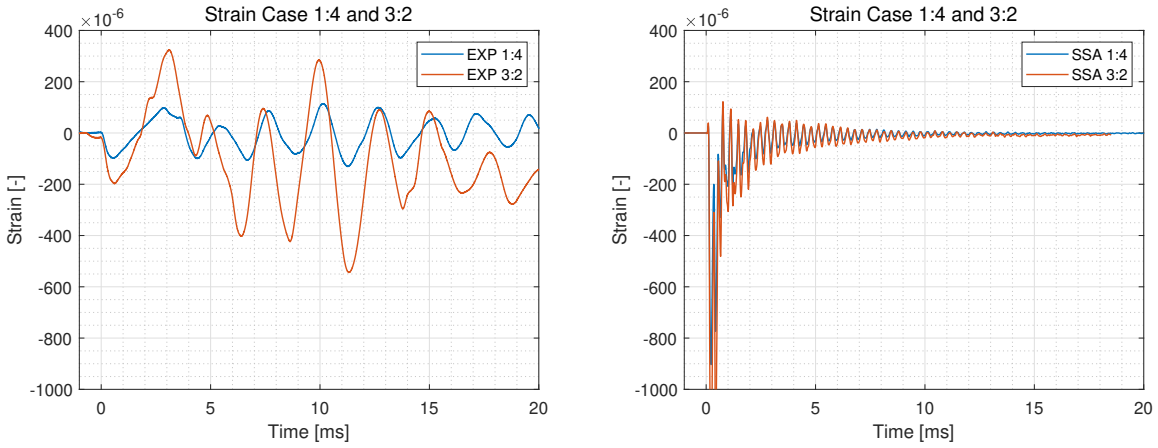

Fig 6.5: Strain responses at the top of the cylinder for a) Experiments and b) SSA. Case 1:4 and 3:2 are compared.

The oscillations in the response from SSA have a frequency around 3 330 Hz and a natural frequency for the cylinder was found at 3 327 Hz. SSA has probably triggered this natural frequency which was not observed in the experiments. This is because the frequency corresponds to a dry condition and it is therefore once again proven that responses can be received with SSA which are not accurate to a condition under water. The high frequent oscillations are also found because the cylinder is modelled as one body, as the nodes are coupled at the points where the pipe meets the ends. Thus neglecting dampening effects obtained for the experimental cylinder.

The ends of the experimental cylinder are fastened with O-rings, thus a contact condition is present between the ends and the pipe. By modelling the cylinder with contact condition instead of coupled nodes, a better physical representation is given in the model and the response can be more accurate. The first model of the cylinder was created before the construction of the experimental cylinder was finished. Simulations were also run before the experiments. Thus the model can be further improved after the experiments have been executed and the conditions are known.

A new model of the cylinder is created to include a contact condition and a block to represent the accelerometer is also included. The new model of the cylinder is run for Case 1:4 and compared to the first cylinder in Fig 6.6 for the top strain gauge. The response deviate and the magnitude for the model with contact is lower compared to the old model with coupled nodes. It is therefore of high importance how a structure is modelled since it affects the responses. By modelling the contact, the strain response is lower and therefore closer to the experiment. There is, however, still reflections within the experiments, which contributes to uncorrelated results. The model can be made more accurate by modelling the O-rings, wires to the bottom of the pool and the hose with the cables. Each component has a potential to can improve the results.

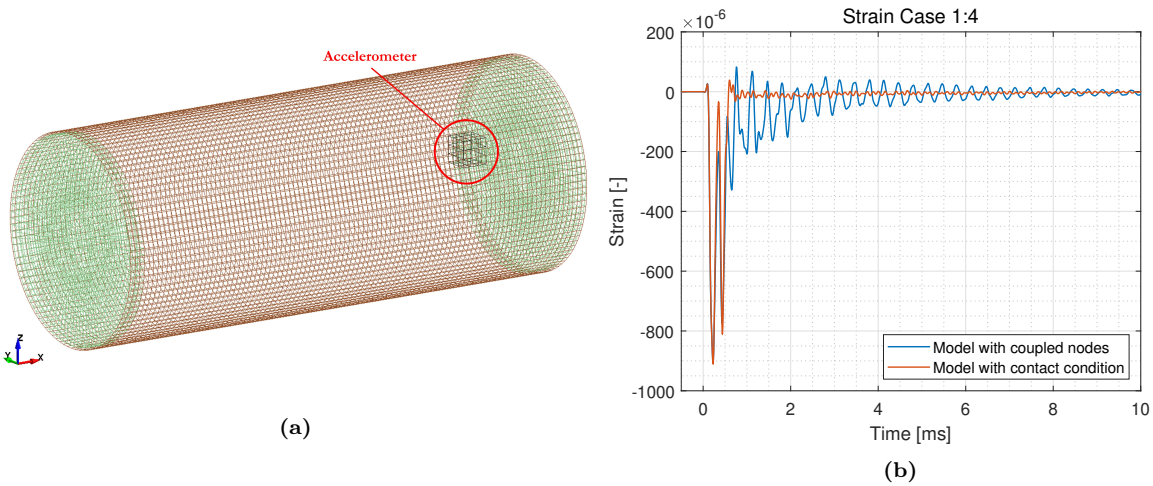

Fig 6.6: a) The model with contact condition and accelerometer and b) the result for the coupled node model compared to the contact condition model.

6.3.4 Bubble impact for Case 1:5

For Case 1:5, the maximum bubble radius was analytically calculated to be larger than the distance to the cylinder, this was therefore expected for the experiment and simulations but is not found. The experimental result is shown in Fig 6.7 for strains, acceleration and pressure. The vertical lines show when changes in the response occur and are based on the acceleration result. The first line is the shock-wave and the second, only 5 ms after, is a secondary impact from the detonation. Exactly what impacts the cylinder is unknown, but it appears too early after the primary shock-wave to be a bubble response since the maximum bubble radius is expected at 20 ms. This response is also seen in strain where a higher impact on especially top and back appears at the second vertical line. After this, the response becomes more oscillative. The third line at 42 ms represents the pressure pulse from the first bubble collapse. This corresponds to the analytically calculated time for the bubble minimum to occur, which is 43 ms. The response from this collapse is seen both in the acceleration and strain plots. Although it is not as significant in strain, all positions have increased magnitudes. The fourth line represents the second bubble pulse, which has less impact on the cylinder. This is especially seen in the acceleration. For strain, all positions decreases slightly with most impact at the top.

For the pressure response, the first shock-wave is captured at the same time as the other results. A secondary peak is found a bit earlier compared to the other responses. This can be due to a delay of response for strain and acceleration, since those gauges measure changes in the material and structure, while the pressure gauge measures directly in the fluid. The first collapse pressure pulse can be seen at 42 ms, similar to the others. The last collapse pulse, which can be seen in both acceleration and strain is not as notable for pressure.

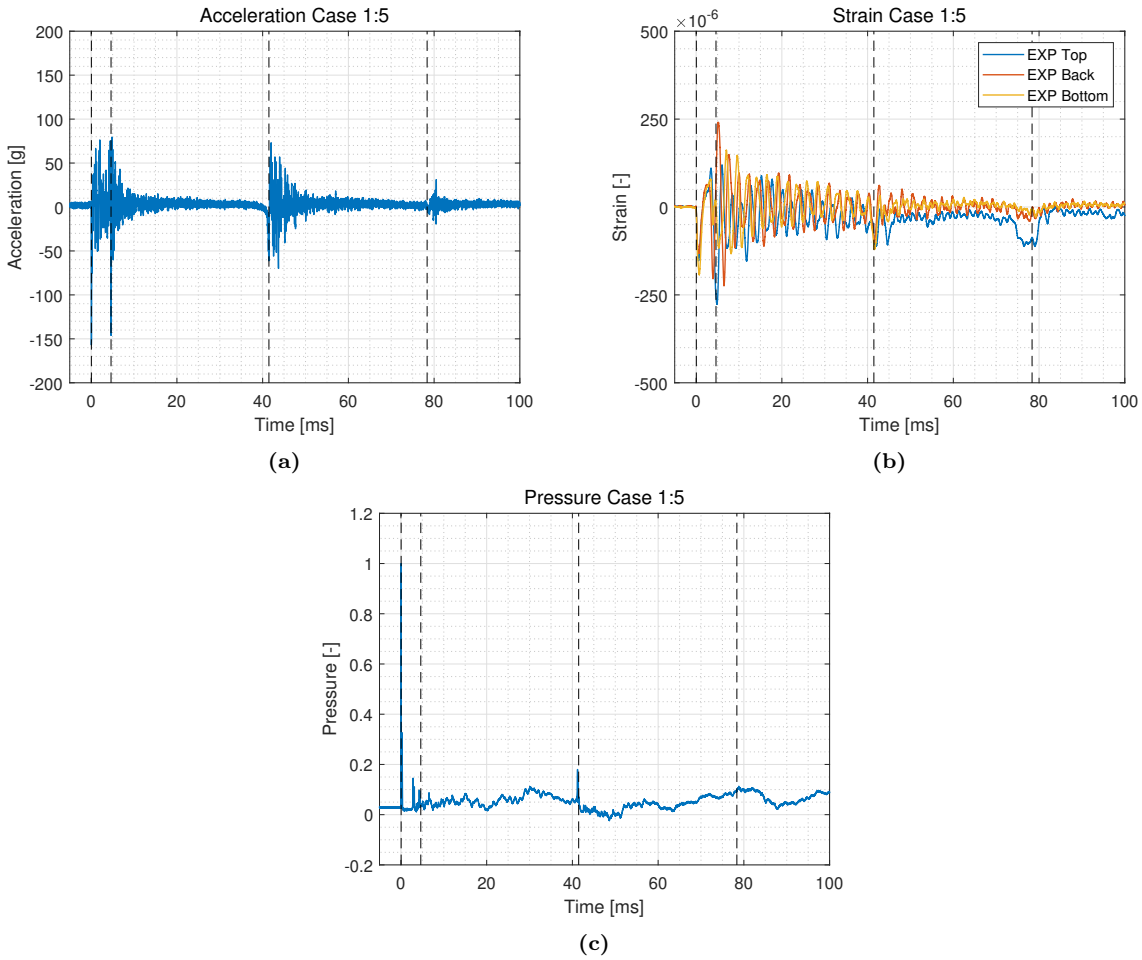

Fig 6.7: Experimental result for Case 1:5 for a) acceleration, b) strains and c) pressure.

The strain response for SSA and S-ALE is shown in Fig 6.8. For SSA, the response from the shock-wave occurs at the same time as for the experiments but no secondary impact can be observed. The highest peak value reaches around -1600×10^{-6} for SSA and is therefore not included in the graph. It is shown that no more than one bubble pulse is found with SSA and the captured collapse appears earlier compared to experiments. The strain responses from S-ALE are very oscillative and irregular, no real pattern or connections can be drawn to the timestamps noted from the experiments. An increase in magnitude happens at 15 ms. The unstable oscillations in the responses from S-ALE are most likely due to a combination of effects from reflections and natural frequencies coinciding. Therefore, only the first milliseconds after the impact of the primary shock-wave are relevant as no reflections have interfered yet. Still, here the magnitude of strain is greater than for the experiments, indicating that the FSI coupling in S-ALE over estimates the applied load to the structure, the same applies for SSA. The magnitude of the response in S-ALE correlates with the peak value of SSA. This shows that SSA is governed by the analytical equations and therefore decreases in magnitude, while S-ALE captures the effects from reflections even though it does not correlate with the experiments.

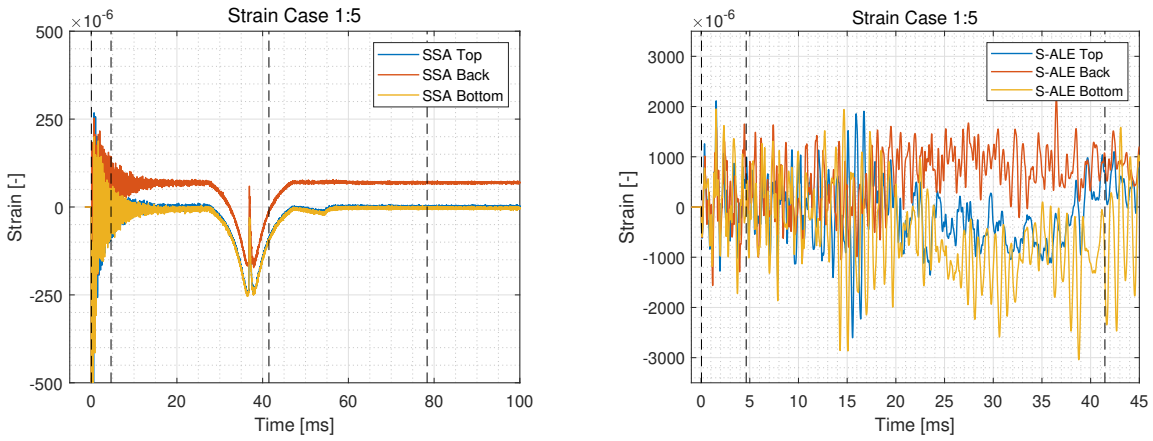

(a) **(b)**

Fig 6.8: Simulated result for a) SSA and b) S-ALE. Observe that the axis is not up to scale between the plots.

As mentioned previously, the bubble was expected to grow past and collide with the cylinder, but that was not the case for either the experiments or simulation with S-ALE. Below in Fig 6.9 can the measured maximum radius from the S-ALE simulation be seen, 0.2 m while a maximum radius of 0.8 m was expected from the analytical expression Eq 2.4.

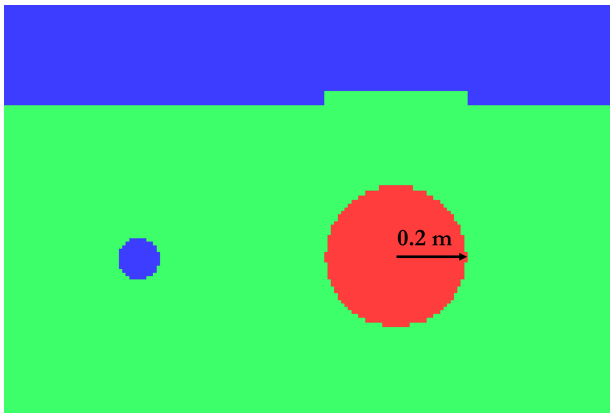

Fig 6.9: Maximum bubble radius reached in S-ALE simulation for Case 1:5

6.3.5 Plastic deformation for Case 2:5

When detonating closer to the cylinder during Serie 2, plastic deformation was expected. This was first found in Case 2:3 with a distance of 0.3 m. There was no measuring system attached for Case 2:3, and the deformation was not particularly distinct. Thus, Case 2:5 is presented instead because the visible deformation was much greater there.

For Case 2:5 in Fig 6.10, it can be seen how the shock-wave affects the cylinder. The distance between the wall of the cylinder and charge point is 0.1 m and from the pictures it is interpreted it takes roughly 0.08 ms for the shock-wave to reach the cylinder. This corresponds to a velocity of 1250 m/s which is in the regime of the value used for speed of sound in the numerical models. After an additional 0.08 ms, deformation from the primary shock-wave can be seen indicating it has already hit the cylinder. It was also noted that the cylinder deformed even more after the impact of the shock-wave. This was due to the collision with the growing bubble. The cylinder deformed to such extent that the ends detached and water filled the cylinder and made it sink to the bottom of the pool.

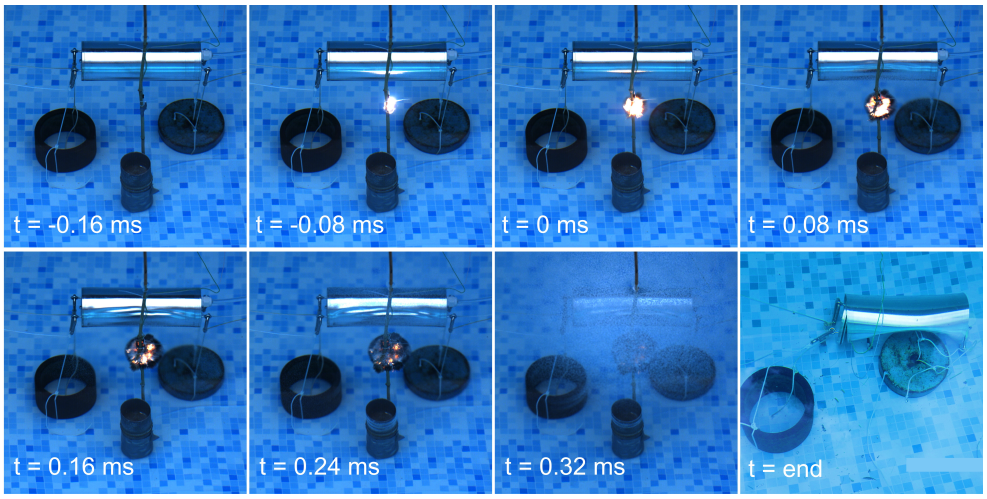

Fig 6.10: Pictures from Case 2:5 when the charge detonates and the cylinder deforms. t=0 is when the shock-wave reaches the front wall of the cylinder.

For SSA, this deformation is not received. The result of the strain with SSA at all positions is shown in Fig 6.11a. After the shock-wave, SSA predicts most strain at the top and bottom of the cylinder. Plastic response is received at all positions and the behaviour differs from earlier studied cases. After the shock-wave, the strain levels out at around 2% and after the bubble collapses, the strain at the front reaches the highest level. The plastic strain needed for damage is 11% for the material used. It is here seen that less than 3% is reached, thus SSA does not predict as distinct damage as found in the experiments. As seen earlier, SSA only applies pressure onto the cylinder instead of the physical impact of a bubble pulsating close to it. How the cylinder is modelled does also impact the damage response. The experimental cylinder with contact allows the ends to rotate and detach for high enough pressure.

In Fig 6.11b, the corresponding results for S-ALE is shown. This simulation was run for a shorter time, because it was know the bubble would be large enough to reach the cylinder. Here the majority of plastic deformation occurs at the front when the primary shock-wave hits the cylinder. The other positions experience less plastic deformation. The front position for S-ALE reaches higher strain than the front for SSA from the primary shock-wave, but other positions for SSA have similar levels of strain from the primary shock-wave as S-ALE has at the front. The distribution of plastic deformation is more accurate for S-ALE when comparing with to the experiments for the primary shock-wave. Showing that the FSI coupling is better at applying loads from a close proximity UNDEX compared to SSA. No additional deformation is received when the bubble reaches the cylinder, this is not what was expected with regards to what the experiments showed in Fig 6.10.

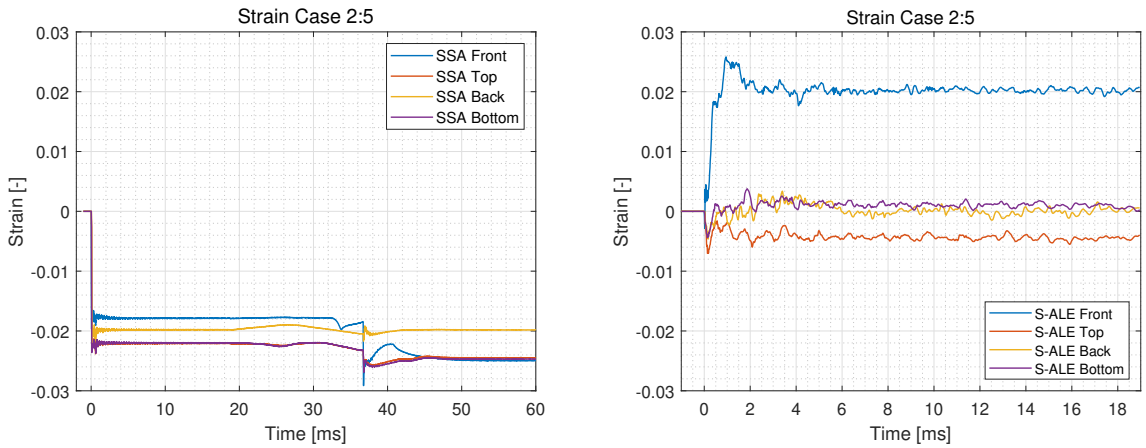

Fig 6.11: Strain responses for Case 2:5 with (a) SSA and (b) S-ALE.

When examining what happened to the cylinder in the S-ALE simulation, it was found that the growing bubble pushes and moves the entire cylinder instead of colliding with it. This is partly due to the cylinder only being locked in z-direction and perhaps having less inertia in the simulation than in the experiments, thus being easier to move. This does not happen in the result for SSA.

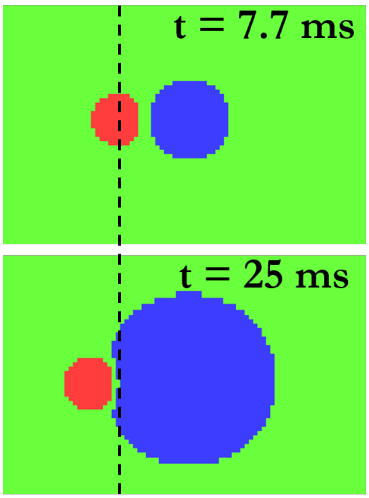

Fig 6.12: Pictures from Case 2:5 when the charge detonates and the cylinder deforms. t=0 is when the shock-wave reaches the front wall of the cylinder.

6.3.6 Further implementation of SSA

A box with acoustic elements is studied with SSA and compared to result for a normal SSA setup and with a gradually larger box of S-ALE elements. As the box of S-ALE elements was smaller for this application compared to the full S-ALE model, the computational cost for this approach was significantly smaller. The strain response at the top is shown in Fig 6.13a and differs where the acoustic elements contributes to a more oscillative behaviour. The frequency is slightly lower for the model with acoustic elements. The model with a S-ALE domain behaves differently. A large positive peak of strain is received just after the shock-wave impact. Also, a sudden positive strain occur at 4 ms and it is interpret that reflections and instabilities that occur in the S-ALE domain after the shock-wave affects the result. In order to receive stable result with S-ALE, a larger domain has to be used. The peak in strain seen at 4 ms for S-ALE does however not affect the acceleration. Thus, there is no bubble pulse or similar that impacts the whole structure.

Acceleration levels are also studied for the different SSA implementations, seen in Fig 6.13b. For the acceleration with SSA compared to acoustic elements, there is a smaller deviation but the general behaviour is similar. The S-ALE domain has responses of higher frequencies and is damped more compared to the other models. This shows that the inclusion of multi-physics through S-ALE works and that the surrounding water dampens the magnitude. The higher frequencies of the oscillations for S-ALE can be caused by a natural frequency of the cylinder submerged in water being hit or the unsteadiness that occur in the domain after the primary shock-wave hit.

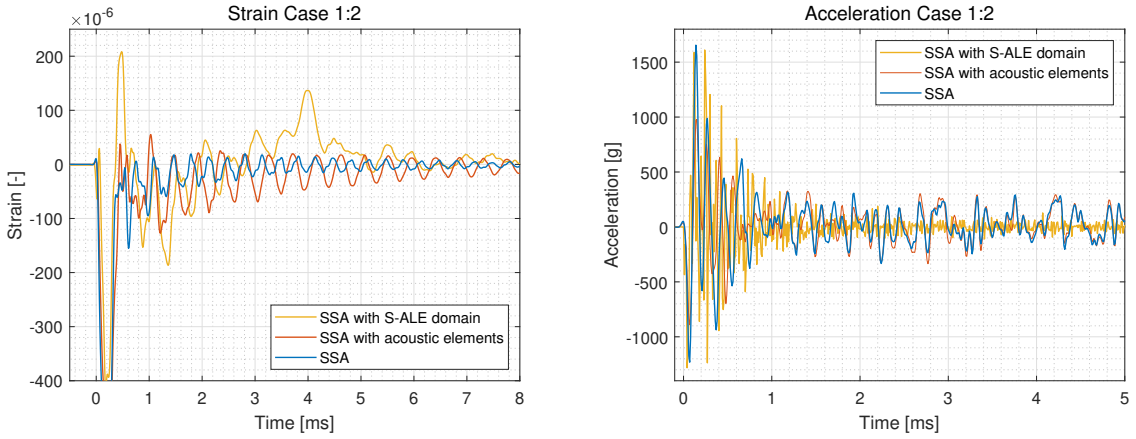

(a) (b)

Fig 6.13: Responses at the top of the cylinder for a) strain and b) acceleration for SSA combined with S-ALE, SSA with a box of acoustic elements and only SSA.

6.3.7 Studied modelling approaches for Case 3:3

For the last presented result, the three base approaches for modelling an UNDEX is compared for Case 3:3. These are SSA, Multi-physical analysis with SSA (SSA + S-ALE) and Multi-physical analysis with full detonation process (S-ALE).

The acceleration levels were measured during the experiments and simulated. Below in Fig 6.14, a comparison between the acceleration levels solved for Case 3:3 and corresponding experiment is seen. The simulation results and experimental results are plotted separately as they differed a lot in magnitude. In Fig 6.14a, the result from SSA is oscillative and has a higher frequency compared to S-ALE, SSA also have higher peak values. The results for SSA combined with S-ALE have a similar high frequency behaviour as normal SSA but the peaks are lower. The reason for S-ALE having lower frequencies in the responses is likely due to how the load from the UNDEX is applied onto the cylinder. For both SSA and SSA combined with S-ALE, the load is applied directly on the cylinder through *LOAD_SSA, while for S-ALE this is done trough the FSI coupling. This indicates that the FSI coupling takes the inertia from both the cylinder and surrounding water into account, thus making it harder to put the cylinder in motion.

Both SSA and S-ALE continues to oscillate while SSA combined with S-ALE and the experimental results stabilizes after the initial shock-wave, as can be seen in Fig 6.14b. A sudden peak can be seen just before 3 ms for the experimental results, this is most likely due to a surface or bottom reflection. That SSA combined with S-ALE stabilizes after the initial shock-wave indicates that the water modelled around the cylinder works as a dampener. This effect is however not received for just S-ALE despite it modelling water around the cylinder as well. This is likely due to reflections from the UNDEX in the domain or that more natural frequencies for the cylinder have been triggered.

The magnitude of the acceleration is higher for the simulation results compared to the experimental. This difference is due to multiple variations and simplifications made in the simulation model compared to the experiments. The dominant one of these is believed to be the modelling of the cylinder in the simulation models. As mentioned previously, there are differences between the modelled cylinder and the one used for experiments. This allows for some of the shock-wave energy to be absorbed by displacing components in relation to each other, thus dampening the acceleration for the experiments. Another reason the simulation results achieve high responses is that the simulation model gives a numerical solution that captures very rapid and sudden behaviours. Such rapid responses are in reality not possible because of external physical factors and dependencies on other physics. This is supported by the fact that SSA models the least amount of physics and thus gives the highest discrepancies.

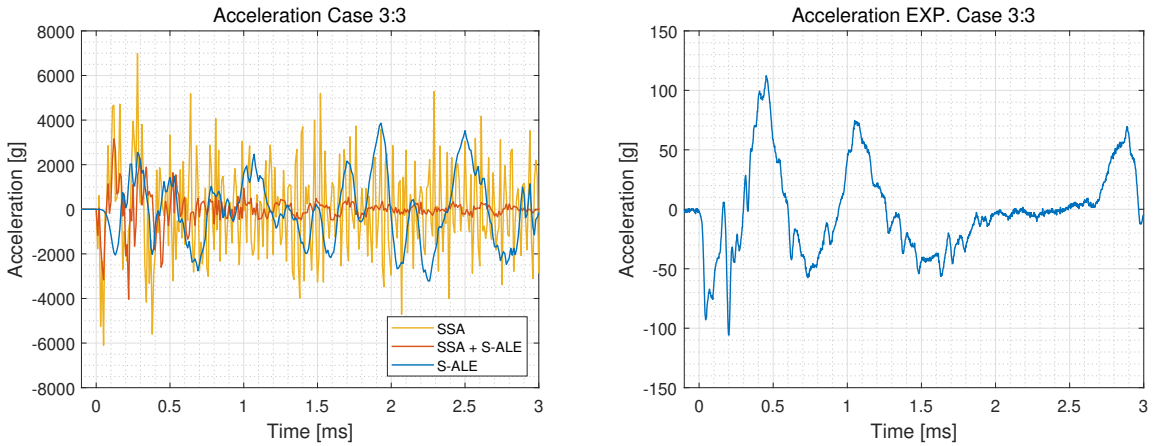

(a) **(b)**

Fig 6.14: a) Acceleration levels at a node on the cylinder end according to simulations with SSA and S-ALE. b) Acceleration levels given by an accelerometer during experiments.

For Case 3:3 the strain at the top of the cylinder was also studied for different modelling methods and compared to experimental data, this can be seen in Fig 6.15. Here it becomes even more apparent that all modelling methods give responses with higher frequencies compared to experiments, supporting the fact that the load application happens faster in the simulations and the inertia of the cylinder and surrounding water is taken less into account. S-ALE responses are also here oscillative with a high frequency due to shock-wave reflections and natural frequencies. The strain responses from SSA and SSA combined with S-ALE behave similarly initially when the load is applied. SSA combined with S-ALE does however continues to oscillate while normal SSA stabilises down, this is likely due to the added physics of water surrounding the cylinder.

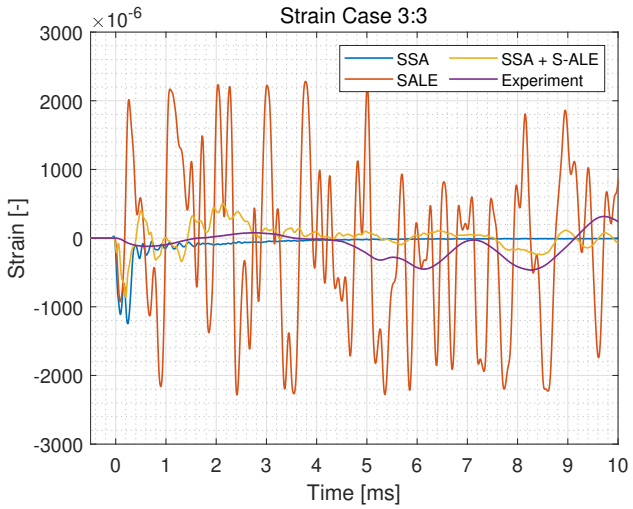

Fig 6.15: Tangential strain at the top position of the cylinder for Case 3:3, all modelling methods and experiments.

7 Conclusions and Future work

Conclusions of the work and suggestions of future work are presented.

7.1 Conclusions

Studies have been performed for two different methods of modelling an UNDEX. Earlier work has been used to conclude that the added mass method used to obtain wet natural frequencies is not fully applicable, since it will trigger new behaviours due to increased density. In this study, it was concluded that SSA does not take the damping effects of water into account. This lead to dry natural frequency oscillations for SSA, which did not correspond to the experimental results.

It has been shown that SSA only applies the pressure of a primary shock-wave and only the first bubble pulse. If a detonation is initiated close to the object, that the bubble should directly impacts the structure, this will not be captured by SSA. The strain response was improved by including acoustic elements, but it did not affect the acceleration.

The implementation of S-ALE was harder than expected but a model was completed that worked to some extent. Using ambient boundary conditions does not work as non-reflective boundaries and reflections at domain boundaries are still present. A cell size two times the explosive charge diameter is enough to resolve detonation and shock-wave propagation. A better refined mesh or larger explosive charge would improve the agreement to experimental results. Due to more physics being included the S-ALE model gives a better representation of the interaction between shock-wave and structure, giving results better in line with experiments. The SSA combination with S-ALE proved for some aspects to perform better than just SSA and on the same level as S-ALE while still being cheaper to compute than a full S-ALE model.

Lastly, it can be concluded that there are multiple aspects which effects the result from experiments and in order to receive correlating result from numerical models, it is important to model the structure and fluid domain as accurate as possible. It would be beneficial to improve the experiments with a larger water domain, to decrease the impact of reflections. The numerical models are also sensitive when modelling weak structures together with small charges. It has to be further studied for more robust structures where high frequent oscillation does not occur and therefore simulations could possibly correlate better with experiments. This was done by Sjögren [7] with a larger structure with high weight of charge. He did not receive high frequent oscillations as for the thin walled cylinder used.

7.2 Future work

To be able to improve the numerical models, suggestions for future work are presented and these are:

- Accurate model of test object

  How the structure is modelled affects the result and it is therefore important to be considered for the desired accuracy.

- Experiments

  Perform new experiments with larger water domain and stiffer structure with thicker wall, to receive less oscillations and reflections in the experiments. Executing experiments with

a larger explosive could be beneficial, as the results would be of higher magnitude and therefore less sensitive to disturbances from external factors. It would also be interesting to capture the full detonation under water to validate it with the data and confirm how the structure was impacted.

- SSA

  The method should be further studied with larger distance and weight of charge. A stiffer structure would probably also improve the result. Increasing the accuracy of natural frequencies by applying mass on the structure without modifying the material properties.

- S-ALE

  Implementation of new *keywords* that are made for S-ALE and check that they give results that agree with the old ALE *keywords*. Evaluate other methods for BCs to remove the effects from domain boundary reflections. If the amount of explosive material is increased the pressure distribution can be improved or mesh be made coarser and less computational heavy. There are also possibilities to further refine/coarsen the mesh to make simulations more efficient.

References

[1] Costanzo FA. Underwater Explotion Phenomena and Shock Physics. Naval Surface Warfare Center Carderock Division, UERD; 2010.

[2] Reid W. The Response of Surface Ships to Underwater Explotions. DSTO Aeronautical and Maritime Research Laboratory; 1994.

[3] Alfredsson B. Handbok och formelsamling i Hållfasthetslära. Instutitionen för Hållfasthetslära KTH; 2018.

[4] LS-DYNA. Theory manual. Livermore Software Technology Corporation; 2006.

[5] Sarpkaya T. Transverse oscillations of a circular cylinder in uniform flow, Part-I. Naval postgraduate school Monterey, California; 1977.

[6] Webster K. Investigation of Close Proximity Underwater Explosion Effects on a Ship-Like Structure Using the Multi-Material Arbitrary Lagrangian Eulerian Finite Element Method. Virginia Polytechnic Institute and State University, Virginia, USA; 2007.

[7] Sjöstrand E. Structural Analysis of Underwater Detonations; 2021. `http://ltu.diva-portal.org/smash/get/diva2:1562415/FULLTEXT01.pdf`.

[8] Otsuka M, Matsui Y, Murata K, Kato Y, Itoh S. A study on shock wave propagation process in the smooth blasting technique. 8th International LS-DYNA Users Conference. 2004.

[9] LS-DYNA. Keyword user's manual; 2021.

[10] Nawa N, Just T. Dynamische Einwirkungen auf Stahlstrukturen - Simulation einer Ansprengung auf eine mögliche U-Bootstruktur. DYNAmore GmbH; 2004.

[11] Lindgren J, Karlsson H. Fluid-structure interaction. Division of Structural Mechanics, LTH; 2017.

[12] Özarmut B. Fluid-Composite Structure-Interaction in Underwater Shock Simulations. Thyssenkrupp Marine Systems GmbH; 2019.

[13] Chen H. LS-DYNA Structured ALE (S-ALE) Solver. International LS-DYNA Users Conference. 2016. Available from: `https://www.dynalook.com/conferences/14th-international-ls-dyna-conference/simulation/ls-dyna-r-structured-ale-s-ale-solver`.

[14] LS-Dyna. Defense applications with focus on blast and explosives. Dynamore Nordic AB; 2021.

[15] Candia SD, Ojeda R, Reid W, Ratcliffe M. The Whipping Response of a Submerged Platform Subjected to Near-field, Non-Contact Underwater Explosions. Australian Government, Department of Defence: Science and Technology; 2018.

[16] Monterrubio L, Krysl P. Natural frequencies of submerged structures using an efficient calculation of the added mass matrix in the boundary element method. Journal of vibration and acoustics. 2018.

[17] Balduzzi F, Bianchini A, Ferrara G, Ferrari L. Dimensionless numbers for the assessment of mesh and timestep requirements in CFD simulations of Darrieus wind turbines. Elsevier. 2016.